Article type : Original Manuscript

Internal architecture of mass-transport deposits in basinal carbonates:

A case study from southern Italy

D. JABLONSKÁ[*], C.N. DI CELMA[*], E. TONDI[*], G.I. ALSOP[†]

** School of Science and Technology - Geology Division, University of Camerino, Camerino 62032, Italy. (E-mail: danica.jablonska@unicam.it)*

[†] *Department of Geology and Petroleum Geology, School of Geosciences, University of Aberdeen, Aberdeen AB24 3UE, UK*

Associate Editor – Christian Betzler

Short Title - Mass-transport deposits within basinal carbonates

This article has been accepted for publication and undergone full peer review but has not been through the copyediting, typesetting, pagination and proofreading process, which may lead to differences between this version and the Version of Record. Please cite this article as doi: 10.1111/sed.12420

ABSTRACT

Submarine mass-transport deposits represent important stratigraphic heterogeneities within slope and basinal sedimentary successions. A poor understanding of how their distribution and internal architecture affects the fluid flow migration pathway, may lead to unexpected compartmentalization issues in reservoir analysis. Studies of modern carbonate mass-transport deposits mainly focus on large seismic-scale slope failures, however the near-platform basinal depositional environment often hosts mass-transport deposits of various dimensions. The small scale and mesoscale (metres to several tens of metres) carbonate mass-transport deposits play a considerable role in distribution of sediment and therefore have an impact on the heterogeneity of the succession. In order to further constrain the geometry and internal architecture of mass-transport deposits developed in near-slope basinal carbonates, a structural and sedimentological analysis of sub-seismic-scale mass-transport deposits has been undertaken on the eastern margin of the Apulian Carbonate Platform in the Gargano Promontory, south-east Italy. These mass-transport deposits, that locally comprise a large proportion (50 to 60%) of the base of slope to basinal sediments of the Cretaceous Maiolica Formation, typically display a vertically bipartite character, including debrites and slump deposits of varying volume ratios. A range of brittle and ductile deformation styles developed within distinct bed packages, together with the presence of both chert clasts, folded chert layers and spherical chert nodules, suggests that sediments were at different stages of lithification prior to downslope movement associated with mass-transport deposits. This study helps elucidate the emplacement processes, frequency and character of sub-seismic-scale mass-transport deposits within the basinal carbonate environment, and thereby reduces the uncertainties in the characterization of sub-surface carbonate geofluid reservoirs.

Keywords: Basinal carbonates, debris flow deposits, Gargano Promontory, Maiolica Formation, slumps, slump folds

INTRODUCTION

Mass-transport deposits (MTDs) are recognized as one of the most important sediment-inputs of many slope to basin environments (Posamentier & Martinsen, 2011) and form a significant component of many deep-marine sedimentary successions in both active and passive continental margins (Collot et al., 2001; Zampetti et al., 2004; Moscardelli et al., 2006; Lamarche et al., 2008; Gamboa et al., 2010; Principaud et al., 2015). Mass-transport deposits are the result of mass-wasting events triggered by gravitational instability of the shelf-edge and slope staging areas, and comprise a spectrum of end-member deposit types, such as slides, coherent and incoherent slumps and debrites (Pickering, 1987; Moscardelli & Wood, 2008; Posamentier & Martinsen, 2011). The dimensions of individual MTDs may vary significantly, with downslope lengths ranging from tens of metres to several hundreds of kilometres, and thicknesses ranging from several metres to thousands of metres (Haflidason et al., 2004; Alves, 2010; Dykstra et al., 2011; Moscardelli & Wood, 2015). Recurrent mass wasting and downslope translation of material may occur along slopes with gradients of less than 1º (Haflidason et al., 2004), and creates submarine scars and depositional topography that shape the underwater morphology of basin margins. Mass-transport deposits may also control the distribution and geometry of younger turbidite reservoirs (Armitage et al., 2009; Kneller et al., 2016) and can be used to constrain the timing and style of contractional deformation within developing deep-water fold and thrust belts (Ortiz-Karpf et al., 2017).

Over the last decades, several outcrop studies focusing on the internal architecture of MTDs have been undertaken in order to investigate processes occurring during the transport and emplacement of the failed material. These studies, which have mostly been carried out in siliciclastic systems and only rarely in carbonate systems (Pickering, 1987; Lucente & Pini, 2003; Pickering & Corregidor, 2005; Butler & McCaffrey, 2010; Van Der Merwe et al., 2009, 2011; Ogata et al., 2014), indicate that MTDs move along a basal detachment surface that may either follow the bedding plane (Strachan, 2002; Van Der Merwe et al., 2011) or plough through the underlying beds incorporating the underlying material into the moving mass (Strachan et al., 2008; Ogata et al., 2012; Sobiesiak et al.,

2016). Internally, gravity-driven soft sediment deformation processes result in the formation of an array of structures including dip-slip and oblique-slip normal faults (Alsop and Marco, 2012), extensional sedimentary fissures in the upper extensional head (Winterer et al., 1991; Strachan, 2002; Moretti & Spalluto, 2007), and folds, thrusts, ramps and erosional surfaces in the lower compressional part. Also, because mass transport is a complex process, a gradual transition between its component deposit types is very common, resulting in rather composite internal architectures of the final deposits.

This field-based outcrop study focusses on a series of sub-seismic-scale MTDs occurring within the slope and basinal sediments of the Cretaceous Maiolica Formation exposed along the eastern and north-eastern margins of the Apulian Carbonate Platform in the Gargano Promontory, southern Italy (Fig. 1; Cobianchi et al., 1997; Bosellini & Morsilli, 2001; Owen et al., 2011; Jablonská et al., 2016; Morsili et al., 2017). The studied carbonate succession represents a good analogue for the deeply buried hydrocarbon plays discovered in different settings and stratigraphic units along the eastern margin of the Apulian Carbonate Platform, or below the Apennines thrust belt along the western margin of the same palaeogeographic domain (Holton, 1999; Bartello et al., 2008; Cazzini et al., 2015). Accordingly, the results stemming from this study can help to reduce uncertainties in the characterization of similar subsurface carbonate reservoirs. The principal aims of this paper are: (i) to document the frequency of the mesoscale MTDs within the near-slope basinal succession; (ii) to examine the geometry and internal structure of deep-water carbonate MTDs; and (iii) to describe the character of sediments before and after their downslope translation.

GEOLOGICAL AND STRATIGRAPHIC SETTINGS

The Gargano Promontory, eastern southern Italy (Fig. 1), comprises a 3 to 4 km thick portion of Triassic–Eocene carbonates and evaporites deposited on a Permian to Triassic basement that is documented from prospect wells (Martinis & Pavan 1967; Bernoulli 1972; D'Argenio, 1976; Borgomano & Philip, 1987; Luperto Sinni & Masse, 1987; Bigazzi et al., 1996; Graziano, 1999;

Bosellini et al., 1999; Borgomano, 2000). The most important depositional phases occurred during and after breakup of the Tethyan Mega-platform by Early Jurassic extension. Fragments of this mega-platform, comprising smaller shallow-water platforms separated by pelagic basins, continued to grow in western-central Tethys until the Middle Cretaceous (Masse et al., 1993, 1996; Skelton & Gili, 2012; Cazzini et al., 2015). One of the platforms, the Jurassic and Lower Cretaceous Apulia Carbonate Platform, extended from present-day central Italy to western Greece (Chamot-Rooke et al., 2005).

The Apulian Carbonate Platform was surrounded by the Umbro-Marche Basin to the north, the Ionian Sea Basin to the north-east and east; and by the smaller, inner Apula basin to the west (Fig. 2; Pieri & Mattavelli, 1986; Zappaterra, 1990; Morsilli & Bosellini, 1997). In the present, the Gargano Promontory and the Majella Mountain are the only areas where the transition between platform, slope to basin and deep-basin depositional environments of the Apulian Platform crops out on land (Eberli et al., 1993).

During the Late Jurassic to Early Cretaceous, the whole region was located in a tropical arid climate with a palaeolatitude between 10° and 20°N (Stampfli & Kozur, 2006). This favoured rapid growth of the platform and contributed to deposition of hemipelagic and pelagic sediments in the slope and deep-basinal environments (Simo et al., 1993; Coccioni et al., 2006). However, Early and Middle Cretaceous anoxic events hindered the growth of benthic and pelagic biota in the area, which resulted in environmentally induced drowning unconformities (Bosellini et al., 1993, 1999; Bosellini & Morsilli, 1997; Graziano, 2000).

Shallow-water carbonates of the Apulian Platform display a large variety of facies. Closed, smaller environments of the platform are dominated by algal-mud banks with a scarcity of foraminifera. In open environments, bioclastic sands and rudists prevail. The transitional areas are characterized by elevator rudists (Skelton, 1991; Borgomano, 2000). The platform margin facies (Monte Sacro Limestone) is characterized by massive wackestones with stromatactis while the slope successions (Mattinata Formation) are dominated by gravity-driven deposits, such as debrites, graded

calcarenites (with bioclasts of the aforementioned facies), breccias and megabreccias (Bosellini & Morsilli, 1997, Borgomano, 2000). Within a general progradational trend, the near-slope proximal deposits of the Mattinata Formation pass laterally into the more distal deep-basinal deposits of the Maiolica Formation (Fig. 1B; Cobianchi et al., 1997). The Maiolica Formation extended over the Early Cretaceous Tethys domain (Steinmann, 1925). Along the margins of the Tethyan Ocean and in the vicinity of the carbonate platforms, gravitational redeposition processes significantly modified the sediment distribution (Weissert, 1981; Bosellini & Morsilli, 1997).

The Maiolica Formation consists of thinly-bedded pelagic mudstone–wackestone including nodular and continuous layers of chert (Bosellini, 1999). A large number of calcarenites, calciturbidites and gravity-driven deposits interpreted as slides, slumps and debrites are variably interstratified with these deposits (Bosellini, 1993; Cobianchi et al., 1997; Borgomano, 2000). The nannofossil content of the Maiolica Formation is not well-preserved due to its micritic microcrystalline character, affected by recrystallization of the biogenic material. However, in some places *Nannoconus steinmannii* is the best-preserved species in both slumped and undeformed beds. The calcarenites and some debris-flow facies contain large amounts of sponges, bivalves and benthic foraminifera.

About 50% of the stratigraphic thickness of the Maiolica Formation is represented by MTDs, which document recurring instability and failure of the slope (Bosellini et al., 1993). Gravity-driven collapses in the Maiolica Formation were also documented in the Southern Alps along the Northern Tethyan margin (Weissert, 1984). The spatial distribution and direction of movement of MTDs is controlled by the geometry and orientation of the palaeoslope (Bosellini, 1999; Jablonská et al., 2016; Korneva et al., 2016). Within the study area, the Maiolica Formation is affected by both tectonic and gravitational faulting (Korneva et al., 2016).

STUDY AREA AND METHODOLOGY

The southern part of the Gargano Promontory is well-known for its spectacular deposits of platform-slope limestones that form large megabreccias containing shallow-water lithoclasts supported by

finer-grained, shallow-marine bioclastic grainstones and foraminifera mudstones (Morsilli & Bosellini, 1997; Bosellini et al., 1999; Graziano, 2000; Hairabian et al., 2015). These deposits are regarded as the product of repeated collapse of the platform margin, possibly induced by synsedimentary extensional faulting (Graziano, 1999, 2000; Borgomano, 2000).

Field investigations of the current study were carried out at three selected sites, both along the coast and the road between the towns of Mattinata and Vieste (Fig. 1), where outstanding outcrops of the basinal Maiolica Formation are present. These sites were chosen due to the presence of abundant intraformational gravity failure deposits, and the fact that they are reasonably representative of the numerous MTD-stacking zones in the area. Site 1 (Vignanotica Section) provides a large-scale exposure that enables analysis of the depositional relationships of several MTD-types. Site 2 at Monte Barone shows clear examples of distinct internal structures of mesoscale MTDs. Site 3, comprising the Baia di Campi and Testa del Gargano sections, provides a good insight into the partly limited three-dimensional geometry of MTD-related structures.

In order to decipher the internal architecture and transport dynamics of MTDs, collection of field data involved recording fold geometries (hinge trends, plunge, limb orientations, vergence and facing), fault orientation and offset, character and orientation of bounding surfaces, outcrop logging of representative stratigraphic columns, including description of the salient sedimentological attributes, and line drawings from high-resolution 'photopanels' of inaccessible vertical cliffs. Based on the collected data, calculation of the mass movement direction was performed by using an average of the mean axis method, mean axial-planar method, and the mean axial-planar dip method (see Alsop & Marco, 2012, for further details). The measurements and observations of the MTD-related structures allow the establishment of a general evolutionary model for the lower part of MTDs during downslope translation and after cessation of movement. The line-length balancing method was used to restore the original length of the folded strata, and hence to calculate the amount of relative shortening (see Alsop et al., 2017, for further details of the methodology in MTDs).

RESULTS AND INTERPRETATION

The Vignanotica Section (Site 1)

The Vignanotica Section is exposed along an 800 m long and 70 m high, NNE to SSW oriented sea cliff, and comprises an alternating sequence of undeformed, thinly-bedded cherty pelagic limestones intercalated with metre-scale displaced masses of chaotic and folded strata (Figs 3 to 5). Undeformed packages of thinly-bedded cherty radiolarian limestones comprise 2 to 25 cm thick wackestone–micritic beds (Fig. 4A) alternating with 4 to 20 cm thick, laterally continuous chert layers and occasional 15 to 40 cm thick beds of calcarenite and calciturbidites. Within these packages, the chert is present in layers, seldom in the form of lenses and rarely as spherical nodules. The chaotic and folded units, including a spectrum of gravity-induced deposit types ranging from chaotic debrites to incoherent and coherent slumps, have been labelled VGN 1 to VGN 7 from oldest to youngest (Table 1) and represent a major portion (up to 70%) of the exposed stratigraphy.

At the base, individual chaotic and folded units rest on a quasi-horizontal, gently undulated sharp surface (Figs 4 and 5). Locally, this surface cuts downward into the underlying planar beds, incorporating them into the lowest part of the deformed strata as sediment wedges partially taken from the underlying strata (Fig. 6). Directly overlying the basal surface, the chaotic to folded units comprise a matrix-supported conglomerate interval directly overlain by a folded interval (Figs 4B, 5 and 6A). The lower conglomerate is laterally discontinuous and includes both pebbles and cobbles of micritic limestones and chert randomly dispersed in a muddy matrix (Figs 4B and 6A). The upper interval, which is characterized by variable states of disruption and disaggregation, displays chaotic bedding and convoluted layering (Figs 4B and 6A). The two sub-units may grade directly into one another, but are also locally separated by an abrupt, laterally discontinuous undulating contact. Above, folded packages are truncated by sharp, extremely flat surfaces and are overlain either by a package of undeformed beds, or by another package of chaotic and deformed strata (Figs 4 to 6).

The lateral continuity of both deformed and undeformed strata is interrupted three times by vertically oriented intraformational breccia bodies up to 40 m wide and at least 70 m high (Fig. 3: at distance within the section; 100 to 150 m, 250 to 300 m and 410 to 440 m). Texturally, these breccias are characterized by poor sorting and include chaotic, granule to boulder-size intraformational, very angular blocks up to 5 m in diameter. The top of these breccia bodies is not exposed in the studied section. However, where exposed in the Gargano area, they display a dome-like shape. The entire succession is dissected by Cretaceous and younger sets of WNW to ESE and north-east to south-west striking normal faults, and WNW to ESE and north-west to south-east oriented strike-slip to normal-slip faults (Fig. 3).

Unit VGN 1

The VGN 1 unit is a 2.5 m thick semi-coherent package of micrite – wackestone beds (Fig. 4A and B) displaying tight to isoclinal, asymmetrical to overturned folds and well-developed thrust duplexes in the northern part. In the southern part of the exposure, this unit contains gentle folds with 1 m amplitude and 2 m and 10 m wavelength. Along downdip-oriented outcrops (i.e. to the SE), the basal detachment surface cuts the underlying beds with a 5° angle, while the upper surface is flat with truncated folds.

This unit has been interpreted as a coherent to semi-coherent slump bounded at the base by an erosional surface. Gentle to open folds in the most southern part of the exposed section, and overturned folds and thrust duplexes at its northern part, suggest that this MTD flowed from the southern to the northern quadrant.

Unit VGN 2

The VGN 2 unit is composed of a 3 to 4 m thick package of folded beds with pockets of conglomerate in the lower part (Fig. 4) and it is confined by a flat detachment surface at the base and a planar sharp surface at the top (Figs 3 and 4). Folds vary from open upright, to tight overturned with gently

dipping axial planes, to recumbent folds. The general trend of the fold axis is north-east to south-west and the prevalent fold vergence is towards the north-west. In the southern part of the outcrop, the folded micritic and chert beds overlie a variously thick conglomerate horizon. Within the folded package chert beds are highly dismembered, forming laterally discontinuous layers of chert lenses and nodules. At several places along the outcrop, the lowest portion of this unit shows complete disaggregation of primary bedding and the occasional presence of chert nodules. The entire VGN 2 unit is simply overlain by undeformed planar beds. This unit shows a bipartite character of lower debrite and upper very well-developed slump with sheath, overturned and recumbent folds suggesting that the exposed strata represent the distal portion of the MTD.

The disaggregation of the folds (presence of the conglomerate in the bottom) was probably caused by continuous dragging of the transported deposits over the basal plane. Likewise, the dismembered chert beds may be the product of the contrast in bed competence. Their origin may be associated to extension within bed packages during the downslope motion or dragging of the material. The mean palaeoflow direction obtained from folds exposed in the southern part of the outcrop suggests that sediment transport and slumping direction was towards the south-east.

Unit VGN 3

The VGN 3 unit is >1.5 m thick package of conglomerate (Figs 4 and 5) capped by an interval characterized by dismembered folds (VGN 4). The VGN 3 conglomerate includes randomly distributed, angular to sub-angular pebble-sized and cobble-sized clasts of whitish to greyish micrite (Fig. 5A) and chert variably dispersed within a micritized mudstone matrix. The matrix contains fragments of bivalves and sponges. Its overall thickness decreases towards the north, where it is *ca* 0.4 m thick.

Unit VGN 3 is interpreted as a debrite flow. The presence of fossil fragments of slope facies (bivalves and algae) shows that the debrite originated from a more proximal, upslope setting than the slump (which consists of recrystallized fragments of nannofossils and microfossils).

Unit VGN 4

This unit directly overlies VGN 3, is 7 to 10 m thick, and contains tight recumbent folds with amplitudes of more than 6 m. It is separated from VGN 3 by a 5 to 10 cm thick layer comprising chert nodules in a micritic matrix (Figs 4 and 5A). The relatively constant thickness of VGN3 and VGN 4, combined with the only slightly undulating interface between the two intervals suggests that Unit VGN 4 did not exert much erosive force on the underlying VGN 3.

The VGN 3 unit represents a coherent slump. The layer of chert nodules positioned between interval VGN 3 and VGN 4 may represent an interface between two discrete failure events. Taking into account the platform margin and slope provenance of pebbles and cobbles documented within VGN 3, while the overlying slumps are mostly composed of cherty pelagic beds, it is possible that these mass failures originated in different localities along the depositional profile.

Unit VGN 5

The VGN 5 unit is up to 25 m thick and overlays a 10 m thick package of undeformed beds. In the northern part, its internal architecture is similar to that of the VGN 2 unit, with a clast-rich debrite present in the lower portion, and coherent and incoherent slumps in the upper part (Fig. 5B). However, in the southern area, both parts merge as the disintegrated folded beds are almost indistinguishable due to disaggregation of micritic and the chert beds (Fig. 4B). Within the basal debrite, clasts are typically composed of fragments of micrite and chert beds, and spherical chert nodules supported by a mudstone matrix.

The folded interval is more than 10 m thick and contains irregular wedge-like pockets of rip-up clasts of various sizes entrained from the lower unit (Fig. 5B, arrow). The contact between these two units is gradual, with a distinct surface only developed in the most northern portion of the exposed section, where it is characterized by soft sediment deformation structures resulting from overloading.

Since the debrite and the overlying slump deposits are in gradual transition, their vertical juxtaposition is thought to reflect the decomposition from a rapidly decelerating slump and dismembering of folded beds due to friction. The debris, together with trapped seawater entrained during the downslope movement, may result in the debris flow facilitating the entire slump to move downslope.

Unit VGN 6

This unit is 8 m thick and includes a matrix-supported conglomerate interval composed of pebble-size to boulder-size clasts of micrite and rounded chert, overlain by rare folded beds. A clear planar interface between these units was not observed. Below VGN 6, a 0.5 m thick package of undeformed beds is present. However, in the central portion of the outcrop, underlying beds comprise a 2.5 to 5.0 m thick folded interval (Fig. 5C).

The unit is built up by abundant intraformational clasts and disrupted strata. The wedge-shaped character and the adjacent deformed beds (Fig. 5C) suggest a later, second event affecting the deposited debris flow, and even engaging the underlying strata. These originally planar beds that were sheared and locally incorporated beneath the succeeding event of VGN 6 may give an impression that they belong to the slumped unit. A similar case was documented by Van Der Merwe et al. (2011) in the Karoo Basin where debris flows deformed underlying beds and created a gently-folded horizon.

Unit VGN 7

The VGN 7 is a unit of discordant-bed packages displaying an exposed thickness and length of about 10 m and 100 m, respectively. The basal surface truncates the underlying beds and dips very gently to the south, while its top surface is not well-exposed. In some cases, the beds form very gentle folds. The whole unit is composed of beds cut by several truncation surfaces at various angles. The

truncation, together with the discordance of the bed packages, suggests that this unit represents deposition from multiple failure events, although the exact number of the component slides cannot be established.

Monte Barone Section (Site 2)

The Monte Barone Section (MTB) is an 800 m long road cut located in the western part of the Gargano Promontory (Fig. 1). It is composed of nine highly deformed MTDs that display a range of internal complexity and are intercalated with undeformed, well-bedded micritic limestone and occasional lenses of grumeleuse micrite or microbreccia. These MTDs have been labelled MTB 1 to MTB 9 from oldest to youngest (Table 2; Fig. 6A).

The nine MTDs represent distinct sediment wedges of various thicknesses (1.25 m to >6.0 m) and include intervals with folded and faulted beds and debrites (Figs 6 and 7). The dip angles of the undeformed packages overlying the folded and chaotic intervals vary slightly from dip angles of undeformed packages that underlie deformed horizons (Fig. 6D, dashed and dotted lines). After restoration for tectonic tilting (dip angle 7 to 10°) to a quasi-horizontal position (2°), the basal detachment surfaces are sub-horizontal or gently dipping towards the east/north-east, and the upper contacts are usually flat. Internally, MTDs of the Monte Barone Section are disrupted by numerous upslope and downslope facing normal faults. Folds show a variety of styles (upright to recumbent, symmetrical gentle and open to asymmetrical tight and isoclinal), wavelengths vary from 0.5 to 10.0 m and amplitudes are generally less than 3 m (Fig. 8A and B); their hinges are typically gently plunging (up to 5°), although some of them plunge as much as 40°. Within the stratigraphically lower folded intervals (MTB 2 and MTB 4), folds plunge towards the south/south-east. Two sets of fold axis were observed in folded layers in the middle part of the exposed section (MTB 5, MTB 6 and MTB 8) plunging towards the south-east, SSW and towards the north, north-east, whereas the plunge of folded layers in the uppermost stratigraphic position is towards the east/south-east (MTB 9 and MTB 10). Prevalent fold vergence is towards the north-east and intra-

slump thrusts generally dip towards the west, although in detail, dip directions range from south-west to west/north-west (Fig. 8D). Locally, thrusts may exhibit a back-steepening of the thrust system upslope towards the south-west (Fig. 8A).

Undeformed planar beds that underlie and overlie the deformed horizons dip towards the north/north-east and east. The folded intervals and fold structures are cut by the overlying undeformed beds. In some cases, however, the top surface of the MTD is flat, showing minimal rugosity, and is directly overlain by packages of undeformed beds. Two coherent MTDs (MTB 5 and MTB 6) have been chosen for detailed structural analysis because they provide a large quantity of accessible structural data.

Unit MTB 5

This unit is exposed in a 3 m high and 70 m long outcrop, and consists of a folded interval where neither the basal nor the upper surfaces are exposed. Unit MTB 5 is characterized by open asymmetrical folds in the south-western part, and overturned, tight to isoclinal folds in the north-eastern part of the outcrop. These folds are mostly upward-facing and east-verging, with hinges plunging gently towards the south and south/south-west (Fig. 8A and C). The back limbs of the folds show small-scale normal faults and north–south-striking asymmetrical boudins and layer thinning that, taken together, represent clear evidence of extension (Fig. 9A and B). Two sets of high-angle (60° to 70°), intra-layer small normal faults dipping towards the north-east and west/north-west cut the long limbs of folds in the middle and east/north-east parts of the outcrop, respectively (Fig. 8A). The first fault set shows small offsets and the second set of conjugate normal faults cuts thrust planes and contorted beds of micrites and chert at very high angles, with offsets of 0.3 m. Back-steepened thrusts dipping towards the west/north-west (Fig. 8A), show increasing dip angles in a direction up the inferred palaeoslope (Fig. 8A). In the middle portion of the outcrop, deformed beds are laterally disjoined and filled by debris encompassing porous chalky limestone and chert clasts

(Fig. 8A, 40 to 50 m). Structural balancing and restoration of the *ca* 40 m cross-section across MTB 5 reveals at least *ca* 50% shortening during thrust-fault deformation.

The MTB 5 unit has been interpreted as a coherent slump with distinct extensional (boudinage and normal faults) and compressional (folds and thrusts) features. The small-scale normal faults present on the gentle flanks of folds, dip in the same direction as the fold vergence, and represent local extension connected to the downslope movement. The geometry of the thrust planes (flat at their base and steepening up in a downslope direction) indicates that the thrusts developed in the final stages of slumping (Alsop & Marco, 2011). Back-steepened thrusts dipping in a direction opposite to the fold vergence (Fig. 7A) suggest piggyback thrusting within the MTD (Alsop et al., 2017). The orientation of the deformation features induced by MTDs (folds, faults and thrusts) supports the inference that the prevalent movement direction is towards the east.

Unit MTB 6

Unit MTB 6 is a well-exposed folded package more than 4 m thick and cropping out over a 400 m long section. Lithologically, this unit consists of fine-grained micritic beds containing occasional lenses of microbreccia and grumeleuse structures. Chert nodules occur in strata that follow the structure of folded micritic beds. Throughout the section, the amplitude and wavelength of the folds vary from tens of centimetres to a few metres (<2 m). Isoclinal, tight and recumbent folds have been documented in the most north-eastern part of the outcrop, and these are followed by more upright folds in the central and south-western part of the outcrop, where evidence of refolding is also observed (Fig. 8B). Variable orientation of the fold hinges (Fig. 7B) suggests hinge rotation during the transport. Despite the scattered statistical distribution, two predominant directions of fold hinges towards the north-east and south/south-east can be recognized (Fig. 6D).

The axial planes dip mostly upslope towards the south/south-west or north/north-west (Fig. 7D). The majority of folds exhibit bed thickening in the hinges and thinning on the limbs. However some folds show contrary relationships, indicating later refolding (Fig. 8C). Within some larger folds; smaller, disharmonic folds of distinct layers (especially chert layers) are present (Fig. 7D).

Within MTB 6, two distinct intervals, documenting different deformation styles, were recognized (Fig. 7B – indicated by the stars; Fig. 8G). Both intervals are composed of micrite and chert layers, with the lower one characterized by imbricate structures, and the upper portion characterized by folds that are typically small-amplitude and small-wavelength. The majority of folds exhibit bed thickening in the hinges and thinning on the limbs, which is typical for slump-related structures. The north/north-east part of the exposure, together with 0.5 m of overlaying planar beds, are cut by north–south-striking, concave-up normal faults rooting into the basal surface (Fig. 8E). The offset diminishes from 0.3 to 0.1 m as the fault approaches the folded unit, and the fault dip angle diminishes when passing the folded horizon. Similar cases were observed in the south-eastern part of the outcrop. Here, the normal fault passes through the folded horizon and the few decimetres of capping layers (Fig. 8F). The first capping layer displays the largest offset, while the offset decreases in the folded horizon and planar beds above first capping layer. The propagation of the fault occurred along pre-existing slump-related structure (thrust planes at a fold limb).

Unit MTB 6 hosts gravitationally-related thrust faults that are characterized by listric geometries (Fig. 7B) and dip in two predominant sets towards the west/south-west and west/north-west. In the 60 m long contractional section of MTB 6, the amount of shortening accommodated by folding and thrusting reaches at least 30% (Figs 7B and 8G). In the central part of the exposure, MTB 6 contains distinct bed packages composed of micrite and chert layers of very similar ratios. The lower strata of these intervals are characterized by very gentle folds and imbricate structures (Fig. 7B, purple and brown lines; Fig. 8D and G), while upper beds are locally characterized by disharmonic isoclinal, overturned folds of variable vergence and small amplitude (0.1 to 0.3 m; dark blue and cyan lines on Fig. 7B). The combination of thrust faults with open fold-dominated and disharmonic fold-dominated portions leads to identical overall shortening for both deformed bed packages. The sporadically exposed basal detachment surface in the most north/north-western part of the outcrop is flat and almost parallel to the underlying undeformed beds. Truncation of folds in the uppermost portion of MTB 6 is documented in several parts of the outcrop (Figs 7B and 8E). The emplacement of coherent

slumps and debris flow deposits controls the local depositional angle of the directly overlying undeformed beds, thereby resulting in various depositional dip angles along the outcrop.

The MTB 6 unit is interpreted as a coherent slump, with the outcrop exposing its compressional parts (folds and thrusts; Fig. 7B). Normal faults rooted in a basal detachment and cross-cutting the MTD and its immediately overlying undeformed layers suggest post- emplacement reactivation of the MTD.

Distinct packages of intense compressional zones in the MTB 6 slump host intervals displaying different deformation styles, with intervals of imbricated structures in the lower part, and an interval of folds in the upper part (Figs 7B and 8G). Different deformation styles in beds of similar thickness and composition may be a consequence of different stages of lithification in various portions of the slump. Several studies of MTDs document a brittle phase that post-dates the ductile phase of deformation (Strachan & Alsop, 2006, Debacker et al., 2009). The structural features of both packages represent compressional zones within MTB 6 (Figs 7B and 8G), however they feature different ductile structures (gentle folds and thrusts versus overturned folds with short amplitude and short wavelength). Palaeoflow indicators show that the prevalent movement was towards the north-east. The deviation in the direction of these superimposed MTDs (Fig. 6D) may be caused by changes in the palaeoslope morphology produced by the emplacement of older MTDs.

Two distinct groups of MTD-related normal faults were observed. The first group dips downslope and forms during both the last stage of the mass-transport movement, and also during the post-movement stage. The second group of normal faults dips upslope and is related to a post-movement reactivation, probably using previous thrust planes. In some cases, undulating thrust planes indicate later reworking and folding (Fig. 8C).

The orientation of the deformation features induced by MTDs (folds, faults and thrusts) suggests that the prevalent movement direction was towards the east in MTB 5 and towards the east-/north-east in MTB 6.

Baia di Campi and Testa del Gargano Sections (Site 3)

Unit BDC 1

At Baia di Campi, exquisite outcrops of folded strata (BDC 1) and associated packages of undeformed beds are exposed on the two vertical sides of a north-east/south-west trending, 8 m high and 35 m long road cut (Fig. 9A), a 23 m high and >50 m long sea cliff (Fig. 10A), and on a 40 m high exposure within a cavern with collapsed roof. The basal surface of the folded package is exposed only at the sea-cliff outcrop. This surface is undulated and cuts deeply into the undeformed planar beds below. The folded strata display folds that are typically isoclinal to recumbent or, less commonly, overturned with signs of hinge rolling (Figs 9A and 10B). The fold-hinges are gently plunging (<10°) towards the east, ranging between north-east to south-east trends (Fig. 9B). The mean fold hinge trend on the north-west wall of the road cut is towards 120°, and towards 137° on the opposite south-east wall. Folds verge towards both the north and south. However, the prevalent vergence of folds with amplitudes greater than 1 m is towards the south.

Several recumbent folds show a variation of the fold hinge trend in the range of 10° to 20° (Figs 9A and 10D). The thrusts restricted to the folded horizon strike in a NNW–SSE direction, and generally dip towards the ENE (Fig. 10B and E). Sets of small-scale normal faults that are restricted to certain beds or bed packages mostly root into the thrust or basal planes within the slump, and reflect local extensional regimes (Fig. 10D; middle part). North-west dipping and south-east dipping normal faults that cut undeformed capping beds (Fig. 10B) and with their dip angles diminishing towards the base of the folded unit, are exposed on the south-east wall of the road cut. Another set of north-west to south-east striking extensional faults is recognized within layers of a slide block (Figs 9A and 10E), and show the abutting relationship between planar beds and folds of the lower unit. Based on well-established methods (see Alsop & Marco 2012; Alsop et al., 2016), the average trend of

slump transport was calculated to be N009° or N189°, with the generally southerly-vergence of larger fold and thrust structures suggesting a SSW (N189°) flow direction (Fig. 9B). The upper contact of the folded horizon is conformably overlain by undeformed beds. Although the folded horizon is exposed on the two opposite walls of the road cut, which are approximately 7 m apart, it is not possible to correlate the individual structures and, hence, to analyse their geometry in 3D. In the uppermost portion of the exposure, undeformed strata overlying the MTD are disrupted by many extensional features, such as conjugate normal faults and a vertical breccia filling. There is no evidence that these extensional features (normal faults and laterally discordant breccia) propagate down into the BDC 1 and they rather terminate on its upper surface (Fig. 10E). North-east from the breccia, the dip angle of the overlying undeformed beds passes from sub-horizontal attitudes to 15°. In the middle part of the exposure, another intraformational breccia body with sub-parallel vertical walls is exposed. This feature is 35 m wide, at least 40 m high and 60 m long.

Unit BDC 1 has been interpreted as a coherent to incoherent slump. The folded beds are sometimes interrupted by the pockets of conglomerates, especially in the lowest parts. As in previous cases (VGN2; VGN4) this can be caused by the interaction of the dragged material over the surface by enhanced friction.

Despite the fact that in the Baia di Campi section it was not possible to correlate the slump-related structures between the two walls of the road cut, the differences in the mean fold axes orientation on the south-east and north-west walls were still recorded. The fold vergence and thrust dip recorded within BDC 1 suggests a palaeoflow direction towards the north and NNE (Fig. 9B), respectively.

Units TDG1 and TDG 2

The WSW–ENE to west–east oriented Testa del Gargano (TDG) outcrop is situated approximately 500 m further along the road from Baia di Campi, in a stratigraphically higher position. Here, four MTDs, labelled TDG 1 (oldest) to TDG 4 (youngest) are exposed on the two vertical sides of the road cut. However, only two of them, namely TDG 1 and TDG 2, were chosen for detailed description. The TDG 1 incoherent slump, within which the primary stratification is almost completely lost, crops out on a WSW to ENE oriented wall. Following, TDG 2, a semi-coherent slump is exposed on both west to east oriented walls, approximately 7 to 9 m apart (Fig. 9). Two stratigraphically higher, incoherent slumps (TDG 3 and TDG 4) crop out and are cut by a set of north-west/south-east tectonic normal faults. TDG 1, which is a partially folded interval with highly dismembered beds, exceeds 10 m in thickness and its eastward-dipping basal detachment surface is above a layer of lenticular chert clasts (Fig. 11G). The top surface is erosional and covered by a laterally continuous chert layer (Figs 9A, 11A and C). TGD 1 is characterized by occasional folds with east to west and ESE to WNW trending hinges and prevalent NNE vergence. Disaggregated folds are surrounded by a matrix of fine-grained micritic debris with clasts of micrite and chert. The upper part is characterized by a portion of micritic debris with larger, elongated plate-shaped or cigar-shaped pebbles and cobbles or lenses of chert arranged in the beds (Figs 9A and 11A). In the western part of the outcrop, TDG 1 is cut by a set of opposing north-west to sputh-east striking normal faults (Fig. 11G).

Deposit TDG 2 consists of an 8 m thick package of deformed beds and its basal detachment surface rests on a 0.2 m thick layer of undeformed beds covering TDG1. The top surface of TDG2 is marked by an erosional surface overlain by a package of undeformed beds, with a chert layer forming the first deposited bed (Figs 9A and 11B). Slump-related folds are upward facing and show variable geometry and size (tight to isoclinal and overturned to recumbent folds). The hinge directions range from east to SSE on the northern wall of the road cut, and from south-east to SSE on its southern wall (Fig. 9C). Folds broadly verge towards both the east and west; however, larger folds verge towards the east (Figs 9A, 11D and 11E).

Correlating features across the 7 m wide gap between the exposed walls reveals potential changes in the fold structure and geometry, with N07° to N10° variations in hinge orientations of the same folded beds. The mean fold hinge trend on the north-west and south-east walls is towards N120° and N137°, respectively. In both cases, the prevalent fold facing is upright to horizontal. Based on the restoration of the pre-tilted orientation, the mean trend of transport was towards N012° or 192° (Fig. 9C). Both TDG 1 and TDG 2 consist of 'soft chalky-appearing' micrite.

In the Testa del Gargano section, TDG 1 and TDG 2 were interpreted as a highly dismembered incoherent slump and a coherent slump, respectively. The lateral change in geometry of slump-related folds and thrusts across a 7 m wide gap illustrates the spatial (and lateral) heterogeneity of shearing during mass movement. Sets of small, slump-rooted normal faults were formed in the later stages of movement, or soon after the emplacement of the mass-wasting sediments and associated relaxation. The overlying, plastically undeformed beds represent a sliding portion of sediment that has used the top of the slump as a gliding plane. The post-slumping north-west-dipping and south-east-dipping normal faults that cut undeformed capping beds (Fig. 10A) are interpreted as products of the sliding. The palaeoflow direction of TDG 2 has been calculated towards the north (Fig. 9B).

DISCUSSION

Occurrence and frequency of the mass transport deposits

Repetitive collapse of sediments in the periplatform-slope environment are common processes and have been widely documented in Neogene sediments of the Bahama platform and its peri-platform areas (Harwood & Towers, 1988; Mulder et al., 2012; Jo et al., 2015; Principaud et al., 2015) where they constitute vast portions of the stratigraphic section. Several massive collapses of the slope margin occurred in the area, modelling the sea floor and sometimes overlapping the earlier MTDs (Principaud et al., 2015). In the Bahamas, the redeposited chaotic material was the result of platform-margin failures forming scalloped margins. Such features (scalloped margins and megabreccias), are also seen in the southern part of the Gargano Promontory and are testimony to massive margin failures (Bosellini et al., 1993; Hairabian et al., 2015; Morsilli et al., 2017).

The MTDs discussed in this study are characterized by their largely uniform lithological origin (near-slope to basinal carbonates) and dissimilar products of mass wasting. In the eastern and north-eastern part of the Gargano Promontory, the failures affect the limestone of the Maiolica (Bosellini, 1997) and Mattinata formations (Cobianchi et al., 1997) resulting in slumping and debris flows. The MTDs of both the Vignanotica and Monte Barone study sites build up 60% of the exposed section, from which both slumps and debrites represent 30% of the exposed section in Vignanotica section. However, in the Monte Barone Section, the debrites comprise only 10% and slumps 50% of the exposed section. The MTDs of the Testa del Gargano site represent 50% of the exposed section. Since the studied sites are predominantly characterized by slumps which will generally have smaller travel distance than debris flows, the majority of the debrites are expected to be preserved further downslope.

The width of MTDs can be examined only in the Vignanotica section, where they are laterally continuous for several hundreds of metres. However, the exposure does not show the complete

dimension of the MTDs. The widths of MTDs documented in the Bahama area reach several kilometres (Principaud et al., 2015).

With some exceptions, the composition of studied MTDs is limited to the Maiolica Formation, which extends several kilometres upslope (Fig. 1). Therefore, depending on their location, these MTDs did not travel more than 10 km from the depleting zone. At Monte Barone, travel distance was a maximum of 2 km (palaeoflow direction towards the east). Due to the similar orientation of the palaeoflow, it can be assumed that the source areas were at different positions up the palaeoslope.

Internal deformation structures of mass transport deposits

Structures attributed to basal surface

Studied MTDs range from slides to debrites, however composite MTDs formed of debrites-slumps are abundant. Documented MTDs show variously developed contacts with the underlying sediments (Fig. 12). The lower contacts are marked by bed parallel décollements (Fig. 12A), shear horizons and basal shear layers that represent erosive contacts. When the erosive contact is very rugose, pockets of conglomerates may be deposited and preserved in the depressions (Fig. 12B). The basal surfaces occasionally down-cut into the underlying undeformed sediments in the direction of mass movement (Fig. 4G).

In most cases, the downslope movement above the basal surfaces results in the development of metres thick basal shear layers mostly below blocks and slides. The thickness of this layer depends on the thickness of the overlying material (Alves & Lourenço, 2010; Alves et al., 2014). The development of a basal shear layer depends on the competence and shear strength of the basal surfaces and lithological properties (Deptuck, 2007). In the case of small-scale and meso-scale slumps, the shear layers at the base of MTDs are not fully developed, however, the slump–debrite transition and the conglomerates present in the lower portion of the units documented in this study suggest that the dragged material on the basal plane may produce the basal-shear layer (Fig. 12C). The influence of lithological properties is marked in heterogeneous–multi-layered MTDs containing

weaker, less cohesive layers, such as failures of siliciclastic strata with silt or mud layers (Lucente & Pini, 2003; Dumont et al., 2012) or carbonate strata with marly layers (Weissert, 1984). In the meso-scale and large-scale siliciclastic MTDs, the microscopic texture of the folded beds, and that of the immediately underlying beds, is characterized by rotation and translation of grains. This fabric is attributed to poorly lithified loose sediment resulting in independent granular flow (Lucente & Pini, 2003).

Neither weak beds defining lithological change, nor shear fabrics are present at the base of the studied MTDs. At the microscopic level, there is no clear difference between the texture of underlying beds and beds at the base of MTDs. This means either that the unconsolidated slumped beds did not undergo any internal deformation or granular flow, or that microscale foliation did develop but was later overprinted by micritization and was destroyed.

Internal structures attributed to variation of shear

Zones of variable shear may also develop within MTDs (Deptuck et al., 2007; Dumont et al., 2012) leading to local culminations and depressions associated with surging and slackening flow regimes (Alsop & Holdsworth, 2007). At Testa del Gargano and Baia di Campi, this is demonstrated by the variability of the fold axis and thrust orientations within the slump (Fig. 10D and E). The shape and orientation of slump-related structures on each side of the road suggest variability in orientation of these structures by several degrees. This inconsistency may be explained by the occurrence of layer-normal shear within the MTD (Coward & Potts, 1983; Alsop & Holdsworth, 1993; Alsop & Marco, 2011; Dykstra, 2011).

Structures attributed to zones of extension and compression

Locally confined compressional and extensional regimes within MTDs are more obvious within incoherent slumps containing local zones of relative deceleration and relative acceleration (Fig. 7A and B). The transition from pure shear to simple shear can also induce a transition from extension to compression in the same quadrant of a MTD (Dykstra, 2011), which leads to

compressional (thrusts, folds and undulated surfaces) and extensional (boudins and extensional faults) structures within adjacent portions of MTDs. Adjacent zones of compression and extension may also simply relate to second-order flow cells that develop locally during translation of the MTD (Alsop & Marco, 2014). The MTD-related faults show various orientations, but typically strike sub-parallel to the inferred Apulian palaeoslope (Korneva et al., 2016). However, in the same way that the slump-related folds may laterally undergo axis-rotation, the fault planes may show similar behaviour and therefore their orientation should be interpreted carefully (Debacker et al., 2009). The majority of the documented faults are syn-slumping (they are rooted into the basal shear layer and cut a portion or the whole slump body), while some faults are formed during reactivation of the MTD as newly formed or re-used shear planes cutting a portion of overlaying beds (Jablonská et al., 2016).

Depositional processes

Depositional processes in composite mass transport deposits

Composite MTDs include two or more genetically-related deposit types (sub-units) created by the same failure event. The sub-units may be coherent slumps, incoherent slumps and debrites with a range of combination and transition between them. The down-cutting surface, or the incorporation of already cohesive, although not completely lithified, material from below, reveals the erosive character of these MTDs. The vertical and lateral transition between the component deposit types can be gradual as shown by a progressive change in degree of disaggregation (VGN 5; Figs 4B and 5C), or abrupt and marked by a sharp interface (VGN 2 and BDC 1; Figs 10A and 13). The same lithological organization (debrite in gradual transition to slump) was documented by Cobianchi et al. (1997) in the Maiolica Formation exposed at Ischitella (N Gargano).

Formation of pillow-like masses of dismembered chaotic material in the lower part of the composite MTD, and mixing of this dismembered material with entrapped fluids and finer material enabled the MTDs to move at great velocities (Mohring et al., 1998; De Blasio, 2004). Similar examples have also been documented from the Storegga Slide, where underlying silici-calcareous mud mixed with water

acted as the lubricating layer (Haflidason et al., 2004). This lubricating layer facilitates movement of the slide over long distances with relatively high velocities despite very low slope angles (Haflidason et al., 2004). Within the upper part of the composite MTD, the plastic deformation intensifies upwards from the debris-flow deposit. Such horizons, in the Vignanotica and Testa del Gargano sections are well-developed within MTDs of medium thickness (10 to 40 m).

The composite MTDs displaying a sharp boundary between the components suggest that these mass flows evolved in a more complex way, with the shear surfaces entrapping the dismembered material to the folded horizons. Several lines of evidence, such as the erosive base, occurrence of rip-up clasts and large flame structures rising from underlying units, indicate a cohesive basal surface that was maintained by erosion and entrainment of both coherent and loose material from the underlying muddy substrate.

Slumps have the ability to rework the upper part of the underlying debrites and, locally, to produce undulating contacts (Figs 4E and 13A), or partially incorporate the debrite into the slump. In the case of composite MTDs, an abrupt contact can be marked by a layer of chert nodules.

However, the sharp, very irregular contact between coherent slumps and a dismembered horizon may suggest that the failure of the material was coeval and chaotic units originated from the slump (Figs 4A and 13B). Zones of slackening flow and zones of relative acceleration might have contributed to dismembering of the beds of the slumps, especially in the lower part. A similar situation is documented in the case of the gradual transition between the sub-units (Figs 9A and 13C), where the pockets of chaotic material are present in the base of the MTD, or locally occur within the folded beds. In the chaotic material, dismembered beds, containing mostly well-rounded or cigar-shaped clasts are present. Distinct MTDs may be represented by one component, or may be built up by a sequence, comprising a debrite–slump couplet. In the case of coeval failure of the component sub-units, transported material moves at different velocities depending on the coherency of the material and size of the components. Debris flows reach greater velocities, carrying

larger clasts supported by the strength and buoyancy of the muddy matrix. These flows travel furthest and are absent in the most proximal portion of the MTD. During their downslope movement, the various types of extensional and compressional features within slides and slumps may be localized in different parts (both laterally and vertically) (Dykstra, 2005; Strachan, 2008; Alsop & Marco, 2014).

The deformation effect of mass transport deposits on the underlying and overlying beds

Deformation of the underlying beds

Deformation and remodelling of underlying beds by MTDs was documented in the Vignanotica section and in Baia dei Campi section (Figs 5C and 10A). In the Vignanotica section, a debris flow, VGN 6, deformed portions of underlying beds resulting in multiple folding of the VGN 5 strata (Fig. 5C). Along outcrops of limited lateral and vertical extension, such folded intervals can be misinterpreted as a slump interval. A similar example has been described by Van der Merwe et al. (2011) in the Karoo Basin, where a debris flow deformed the underlying unconsolidated beds. In both cases (this study and that of Van der Merwe et al., 2011), the deformation was enhanced by the overburden.

Deformation of the overlying beds

All of the MTDs observed in the study area have extremely flat truncated tops, indicating that they were deposited in zones of sediment bypass and that their tops were eroded and planned off by succeeding flows. Post-failure deformation of large-scale MTDs may result in faulting and differential sagging of the overlying undeformed material (Alves & Cartwright, 2010; Safadi et al., 2017). A similar case was documented in small-scale and meso-scale MTDs in this study. The post-failure relaxation or remobilization resulted in deformation of few overlaying beds and development

of small-scale, low-angle normal faults (Fig. 8E and F) that strike perpendicular to the direction of the palaeo-movement.

State of the material prior gravity-failure

The degree of sediment lithification in ancient MTDs is not possible to quantify. However, it is possible to estimate the relative degree of lithification by recording the soft-sediment deformation features and comparing them with the observations of modern sediments (Maliva, 2009). Coherent and semi-coherent small-scale to medium-scale slumps composed of micrite and chert beds (2 to 20 cm thick) and rarely of calciturbiditic beds (20 to 40 cm thick) display a range of plastic to ductile deformation features. Some debrites contain material that may derive from the partial disaggregation and collapse of the slope and near-slope facies (refer to Fig. 5), meanwhile the material carried by all of the examined slumps has a strictly basinal origin (micrites). The variability of sediment may influence the diagenesis. However, complete lithification depends on many factors, such as lithology of the sediment, grain size, compaction due to overburden, sediment fluid content and geochemical composition of the fluids crystalizing as cements (Tucker et al., 2001; Hüneke & Mulder, 2011).

Lithification stage of micrite and micritic wackestone prior to collapse

Plastic deformation of micritic and wackestone beds within studied MTDs suggest a low degree of lithification. In most of cases, the material was a poorly lithified mainly radiolarian ooze at the time of collapse, as supported by the following lines of evidence:

1 The lime mud has relatively high intragranular and intergranular porosity shortly after deposition reaching up to 60% (Maliva et al., 2009); hence the fluid content is very high and it can be reduced by diagenetic processes (compaction and cementation) to only several percent.

2 Physical compaction of pelagic beds at the time of collapse was limited. This is because the collapsed sediments were only several decimetres to metres thick and they did not reach significant burial conditions. The amount of overburden (several metres) was insufficient for complete compaction. In the case of the near-surface lithification, the deep sea carbonate pelagic muds seem to have poor diagenetic potential (Matter et al., 1975) compared to other carbonate lithologies, mainly because of limited fluid circulation.

3 The pelagic matrix within debris flows during the collapse entrapped vast amount of water that was entrained during downslope movement, and which enabled it to carry boulders in the sediment mass (Fig. 4F).

Lithification stage of chert prior to failure

Deformation style of chert layers, lenses and nodules implies that the chert underwent brittle plastic to fluid deformation during collapse:

1 The presence of angular chert clasts within the debrites indicates that some chert layers have been lithified prior to collapse and later broken. This implies that the material was eroded from the substratum of older, partly lithified layers and incorporated into the MTD during the downslope motion.

2 Conversely, some chert layers have been poorly lithified at the time of slumping, creating spectacular plastically folded chert layers (Figs 8D, 10 and 11). With continuous movement and flow transition from incoherent slumps to debris flows, these folds were dismembered to produce chert nodules organized in continuous folded horizons (as seen in the case of VGN 4; Fig. 5A).

3 Some nodules found in the debrites encompass micrite grains and pebbles that were later chertified. Here, the silicic ooze simply infilled most of the pores and cemented the grains.

Post-failure lithification of the material, difference between siliciclastic and carbonate mass transport deposits

Siliciclastic sediments are typically considered to possess lower diagenetic potential for lithification during early diagenesis compared to carbonates (Brenner et al., 1991). This is largely because the main components of siliciclastic diagenesis are compaction and cementation, while carbonate diagenesis encompasses chemical cementation of *in situ* dissolved carbonates (Matter et al., 1975), even in the early stages at near-surface conditions (Maliva et al., 2009), with circulating fluids and physical and chemical compaction. Early diagenesis in siliciclastic sediments occurs due to cementation, which is dependent on the presence of fluids that are strongly associated with the depositional environment (such as precipitation of authigenic calcite). However, the most efficient cementation occurs after dissolution and alteration of the silica and carbonate grains in the compactional and thermobaric regimes (Brenner et al., 1991). Fluidized features of partially lithified sediments are described mainly from siliciclastics (Strachan, 2002; Strachan & Alsop; 2006), or siliciclastic and carbonate MTDs (Odonne et al., 2011), and comprise sand and mud volcanos, injected dykes or fluidized basal layers that are almost absent in the studied gravity-driven failures. This suggests a low contrast in bed competence within MTDs and within overlying sediments at the time of collapse and shortly thereafter.

Different deformation styles within distinct slump portions

Within some slumps, different deformation styles influence successive bed portions during the compression. Upper bed packages display small-amplitude, small-wavelength folds suggesting more plastic-like deformation, while lower beds are more likely to be cut by thrusts (Fig. 8G). This pattern repeats along several slump horizons, suggesting different mechanical properties of the distinctive rock package. In the case of micrite layers with no difference in lithology, the various deformation styles reflect different stages of lithification for the certain portion. The thickness within the folded horizon does not vary significantly, and for this reason, the influence of the bed thickness on different deformation styles may be excluded. Uneven deformation styles may be caused by various

lithification potential of the beds (Matter et al., 1975), which can be caused by excessive water content.

CONCLUSIONS

This study provides an insight into the character of mass-transport deposits (MTDs) and their distribution within the basinal Lower Cretaceous Maiolica Formation in the Gargano Promontory of southern Italy. Mass transport deposits represent a significant portion of the studied succession reflecting the long-term instability of the Apulian carbonate platform slope. The field observations and structural data collected from the MTDs enabled the description of their internal architecture and three-dimensional geometry in this study, and show that:

1 The studied MTDs are very well-developed and display distinct structures produced by soft sediment deformation. The best developed MTDs show a complex, bipartite character because they are composed of debrites and slumps of different volume ratios.

2 Distinct deformation styles (brittle to plastic) within certain portions of the gravitationally deformed succession, together with the presence of both chert clasts and spherical chert nodules within debris-flow deposits, indicates that the transported material was at different stages of lithification prior to movement.

3 There is a lateral change in the orientation of slump structures (distortion of fold axis and axial planes) within MTDs due to internal differential shear within different portions of the slump.

4 Erosional features are lacking because debris-flow deposits in the lower part of the moving masses prevent excessive friction of the overlying slumping material, thereby hindering direct contact with the underlying décollement surface.

5 In terms of emplacement processes, the prevalent palaeoflow direction of the mass-transport events is parallel or sub-parallel to the dip of the carbonate-platform margin. A few exceptions may be caused by the morphology of the slope and basinal floor that would distort the local flow path. The accuracy of the palaeoflow direction may be influenced by the position of the exposure within the overall MTD.

ACKNOWLEDGEMENTS

This work has been supported by Reservoir Characterisation Project (www.rechproject.com) and FAR Project 2014 'Characterisation and modelling of natural reservoirs of geofluids in fractured carbonate rocks', funded by the University of Camerino, coordinator Emanuele Tondi. We acknowledge use of Rick Allmendinger's stereonet programme R. W. Allmendinger © 2006–2014). We would like to express our gratitude to reviewer H. Ortner, an anonymous reviewer, Associate Editor C. Beltzer and Chief Editor P. Pufahl for their precious comments and for their useful suggestions that led to the improvement of the article's quality.

REFERENCES

Alsop, G.I. and **Holdsworth, R.E.** (2007) Flow perturbation folding in shear zones. In: *Deformation of the Continental Crust: The Legacy of Mike Coward.* (Eds A.C. Ries, R.W.H. Butler and R.D. Graham), *Geological Society, London, Spec. Publ.*, **272**, 77-103.

Alsop, G.I. and **Marco, S.** (2011) Soft-sediment deformation within seismogenic slumps of the Dead Sea Basin. *Journal of Structural Geology,* **33**, 433–457.

Alsop, G.I. and **Marco, S.** (2012) A large-scale radial pattern of seismogenic slumping towards the Dead Sea Basin. *Journal of the Geological Society*, **169**, 99-110.

Alsop, G.I. and **Marco, S.** (2014) Fold and fabric relationships in temporally and spatially evolving slump systems: a multi-cell flow model. *Journal of Structural Geology*, **63**, 27-49.

Alsop, G.I., Marco, S., Weinberger, R. and **Levi, T.** (2016) Sedimentary and structural controls on seismogenic slumping within mass transport deposits from the Dead Sea Basin. *Sedimentary Geology* **344**, 71-90.

Alsop, G.I., Marco, S., Levi, T. and **Weinberger, R.** (2017) Fold and thrust systems in mass transport deposits. *Journal of Structural Geology*, **94**, 98-115.

Alves, T.M. (2010) 3D Seismic examples of differential compaction in mass-transport deposits and their effect on post-failure strata. *Mar. Geol.*, **271**, 212–224.

Alves, T.M., Kurtev, K., Moore, G.F. and **Strasser, M.** (2014) Assessing the internal character, reservoir potential and seal competence of mass-transport deposits using seismic texture: a geophysical and petrophysical approach. *AAPG Bulletin*, **98**, 793–824.

Alves, T.M. and **Lourenço, S. D. N.** (2010) Geomorphologic features related to gravitational collapse: submarine landsliding to lateral spreading on a Late Miocene–Quaternary slope (SE Crete, eastern Mediterranean). *Geomorphology*, **123**,13-33.

Armitage, D.A., Romans, B.W., Covault, J.A. and **Graham, S.A.** (2009) The influence of mass-transport-deposit surface topography on the evolution of turbidite architecture: the Sierra Contreras, Tres Pasos Formation (Cretaceous), Southern Chile. *Journal of Sedimentary Research*, **79**, 287-301.

Bernoulli, D. (1972) North Atlantic and Mediterranean Mesozoic facies: a comparison, In: *Initial Reports Deep Sea Drilling Project* (Eds C.D. Hollister and I. I. Ewing) U.S. Government, Washington, 801-871.

Bigazzi, G., Laurenzi, M.A., Principe, C. and **Brocchini, D.** (1996) New geochronological data on igneous rocks and evaporites of the Pietre Nere point (Gargano Peninsula, Southern Italy). *Boll. Soc. Geol. It.*, **115**, 439-448.

Borgomano, J.R.F. (2000) The Upper Cretaceous carbonates of the Gargano-Murge region, southern Italy: a model of platform-to-basin transition. *AAPG Bulletin*, **84**, 1561–1588.

Borgomano, J.R.F. and **Philip, J.** (1987) The rudist carbonate build-ups and the gravity carbonates of the Gargano-Apulian margin (Southern Italy, Upper Senonian). *Mem. Soc. Geol. It.*, **40**, 125-132.

Bosellini, A. and **Morsilli, M.** (1997) A Lower Cretaceous drowning unconformity on the eastern flank of the Apulia Platform (Gargano Promontory, southern Italy). *Cretaceous Research,* **18**, 51-61.

Bosellini, A. and **Morsilli, M.** (2001) Il Promontorio del Gargano: cenni di geologia e itinerari geologici. Quaderni del Parco Nazionale del Gargano, 48.

Bosellini, A., Morsilli, M. and **Neri, C.** (1999) Long-term event stratigraphy of the Apulia Platform Margin (Upper Jurassic to Eocene, Gargano, Southern Italy). *Journal of Sedimentary Research*, **69**, 1241–1252.

Bosellini, A., Neri, C. and **Luciani, V.** (1993) Platform margin collapses and sequence stratigraphic organization of carbonate slopes: Cretaceous–Eocene, Gargano Promontory, southern Italy: *Terra Nova*, **5**, 282–297.

Bracco Gartner, G.L., Morsilli, M., Schlager, W. and **Bosellini, A.** (2002), Toe-of-slope of a Cretaceous carbonate platform in outcrop, seismic model and offshore seismic data (Apulia, Italy), *Geologische Rundschau*, **91**, 315-330.

Brenner, R. L., Ludvigson, G.A., Scal, R. and **Dogan, A. U.** (1991) Diagenetic modeling of siliciclastic systems: status report. Kansas Geological Survey, Bulletin, **233**, p. 123-137

Butler, R.W.H. and **McCaffrey, W.** (2010) Structural evolution and sediment entrainment in mass-transport complexes: outcrop studies from Italy. *Journal of the Geological Society*, London, **167,** 617–631.

Cazzini, F., Zotto, O.D., Fantoni, R., Ghielmi, M., Ronchi, P. and **Scotti P.** (2015) Oil and gas in the Adriatic foreland, Italy. *Journal of Petroleum Geology*, **38**, 255–279,

Chamot-Rooke, N., Rabaute, A. and Kreemer, C. (2005) Western Mediterranean Ridge mud belt correlates with active shear strain at the prismbackstop geological contact. *Geology*, 33, 861-864.

Cobianchi, M., Luciani, V. and **Bosellini, A.** (1997) Early Cretaeous nannofossils and planktonic foraminifera from northern Gargano (Apulia, southern Italy). Cretaceous Research, **18**, 249-293.

Coccioni, R., Luciani, V. and **Marsili, A.** (2006) Cretaceous oceanic anoxic events and radially elongated chambered planktonic foraminifera: paleoecological and paleoceanographic implications. *Palaeogeography, Palaeoclimatology, Palaeoecology*, **235**, 66-92.

Collot, J.-Y., Lewis, K. B., Lamarche, G. and **Lallemand, S.** (2001) The giant Ruatoria debris avalanche on the northern Hikurangi margin, New Zealand: result of oblique seamount subduction, *Journal of Geophysical Research*, **106**, 271-297.

Cossey, S.P.J. (2011) Mass Transport Deposits in the Upper Paleocene Chicontepec Formation, Mexico. In: *Mass Transport Deposits in Deepwater Settings* (Eds R.C. Shipp, P. Weimer and H.W. Posamentier) *SEPM Special Publication*, **96**, 269-278.

Coward, M. P. and **Potts, G. J.** (1983) Complex strain patterns at the frontal and lateral tips to shear zones and thrust zones. *Journal of Structural Geology*, **5**, 383-399.

D'Argenio, B. (1976). Le piattaforme carbonatiche periadriatiche: una rassegna di problemi nel quadro geodinamico Mesozoico dell'area mediterranea. *Soc. Geol. Italiana. Memorie*. **13**, 137-160.

Debacker, T.N., Dumon, M. and **Matthys, A.** (2009) Interpreting fold and fault geometries from within the lateral to oblique parts of slumps: a case study from the Anglo- Brabant Deformation Belt (Belgium). *Journal of Structural Geology*, **31**, 1525-1539.

De Blasio, F. V., Ilstad, T., Elverhøi, A., Issler, D. and **Harbitz, C. B.** (2004) High mobility of subaqueous debris flows and the lubricating-layer model. In: *Offshore Technology Conference*, Houston, TX, 11pp.

Deptuck, M.E., Mosher, D.C., Campbell, D.C., Hughes-Clarke, J.E. and Noseworthy, D. (2007) Along slope variations in mass failures and relationships to major Plio-Pleistocene morphological elements,

SW Labrador Sea. In: Submarine Mass Movements and Their Consequences (Eds V. Lykousis, D. Sakellariou, and J. Locat), pp. 37-45. Springer.

Dumont, T., Schwartz, S., Guillot, S., Simon-Labric, T., Tricart, P. and Jourdan, S. (2012) Structural and sedimentary records of the Oligocene revolution in the Western Alpine arc. J. Geodyn. **56-57**, 18-38.

Dykstra, M. (2005) Dynamics of Sediment Mass-Transport from the Shelf to the Deep Sea. PhD Thesis, University of California, Santa Barbara, 152 pp.

Dykstra, M., Garyfalou, K., Kertznus, V., Kneller, B.C., Milana, J.P., Molinaro, M., Szuman, M. and **Thompson, P.** (2011) Mass-transport deposits: combining outcrop studies and seismic forward modeling to understand lithofacies distributions, deformation, and their seismic expression. In: (Eds H. Posamentier, P. Weimer and C. Shipp) *SEPM Special Publication*, **95**, 293–310.

Eberli, G.P., Bernoulli, D., Sanders, D. and **Vescei, A.** (1993) From aggradation to progradation: the Maiella Platform, Abruzzi, Italy. *AAPG Mem.,* **56**, 213–232.

Gamboa, D., Alves, T., Cartwright, J. and **Terrinha, P.** (2010) MTD distribution on a 'passive' continental margin: the Espírito Santo Basin (SE Brazil) during the Paleogene. *Mar. Pet. Geol.*, **27**, 1311–1324.

Graziano, R. (1999) The Early Cretaceous drowning unconformities of the Apulia carbonate platform (Gargano Promontory, southern Italy): local fingerprints of global palaeoceanographic events. *Terra Nova*, **11**, 245-250.

Graziano, R. (2000) The Aptian-Albian of the Apulia carbonate platform (Gargano Promontory, southern Italy): evidence of palaeoceanographic and tectonic controls on the stratigraphic architecture of the platform margin. *Cretaceous Research*, **21**, 107-126.

Graziano, R. (2013) Sedimentology, biostratigraphy and event stratigraphy of the Early Aptian Oceanic Anoxic Event (OAE1A) in the Apulia Carbonate Platform Margin - Ionian Basin System (Gargano Promontory, southern Italy). *Cretaceous Research*, **39**, 78-111

Haflidason, H., Sejrup, H.P., Nygard, A., Mienert, J., Bryn, P., Lien, R., Forsberg, C.F., Berg, K. and **Masson, D.** (2004) The Storegga Slide: architecture, geometry and slide development: *Marine Geology*, **213**, 201-234.

Hairabian A., Borgomano, J.R.F., Masse, J.-P. and **Nardon, S.** (2015) 3-D stratigraphic architecture, sedimentary processes and controlling factors of Cretaceous deep-water resedimented carbonates (Gargano Peninsula, SE Italy). *Sedimentary Geology*, **317**, 116–136.

Harwood, G.M. and **Towers, P.A.** (1988) Seismic sedimentologic interpretation of a carbonate slope, north margin of Little Bahama Bank. In: Proceedings ODP, Scientific Research (Eds J.A. Austin, W. Schlager, et al.), **101**, 263-277.

Holton, J. (1999) Four geologic settings dominate oil, gas fields of Italy, Sicily. *Oil Gas J.*, **97**, 81–84.

Hüneke, H. and **T. Mulder** (2011) Deep-Sea Sediments. Developments in Sedimentology, **63** Elsevier, New York. 849 pp.

Jablonská, D., Di Celma, C., Korneva, I., Tondi, E. and **Alsop, I.,** (2016) Mass-transport deposits within basinal carbonates from southern Italy, *Italian Journal of Geosciences*, **134**, 30-40.

Jo, A., Eberli, G. and Grasmueck, M. (2015) Margin collapse and slope failure along southwestern Great Bahama Bank. *Sedimentary Geology,* **317**, 43–52.

Kneller, B., Dykstra, M., Fairweather, L. and **Milana, J.P.** (2016) Mass-transport and slope accommodation: implications for turbidite sandstone reservoirs. *AAPG Bull*., **100**, 213–235.

Korneva, I., Tondi, E., Jablonská, D., Celma, C.D., Alsop, I. and **Agosta, F.** (2016) Distinguishing tectonically- and gravity-driven synsedimentary deformation structures along the Apulian platform margin (Gargano promontory, southern Italy) *Marine and Petroleum Geology*, **73**, 479-491.

Lamarche J., Lavenu, A.P.C., Gauthier, B.D.M., Guglielmi, Y. and **Jayet, O.** (2008) Relationships between fracture patterns, geodynamics and mechanical stratigraphy in Carbonates (South-East Basin, France) *Tectonophysics* **581**, 231-245.

Lucente, C.C. and **Pini, G.A.** (2003) Anatomy and emplacement mechanism of a large submarine slide within a Miocene foredeep in the northern Apennines, Italy: a field perspective: *American Journal of Science*, **303**, 565–602.

Luperto Sinni, E. and **Masse, J.-P.** (1987) Données nouvelles sur la stratigraphie et la micropaléontologie des séries carbonatées de talus et de bassins du Crétacé inférieur du Gargano (Italie méridionale). *Rivista Italiana di Paleontologia e Stratigrafia*, **93**, 347-378.

Maliva, R.G., Missimer, T.M., Clayton, E.A. and **Dickson, J.A.D.** (2009) Diagenesis and porosity preservation in Eocene microporous limestones, South Florida, USA. *Sedimentary Geology*, **217**, 85-94.

Martinis, B. and **Pavan, G.** (1967). Note Illustrative Della Carta Geologica D'Italia Alla Scala 1:100000, Foglio 157, Monte Sant'Angelo. Servizio Geologico d'Italia, Roma, 56.

Masse, J.P., Bellion, Y., Benkhelil, J., Dercourt, J., Guiraud, R. and **Ricou, L. E.** (1993) Lower Aptian (114-112 Ma). In: *Atlas Tethys Palaeoenvironmental Maps*: Explanatory Notes (Eds J. Dercourt, L.E. Ricou, and B. Vrielynck), Commission de la carte géologique du monde, 135-152.

Matter, A., Douglas, R.G. and Perch-Nielsen, K. (1975) Fossil preservation, geochemistry, and diagenesis of pelagic carbonates from Shatsky Rise, northwest Pacific. *In* (Eds R.L. Larson, R. Moberly, et al.), Init. *Repts. DSDP*, **32**: Washington (US Govt. Printing Office), 891-921.

Mohrig, D., K. Whipple, C. E. and **Parker, G.** (1998) Hydroplaning of subaqueous debris flows. *Geol. Soc. Am. Bull.*, **110**, 387 – 394.

Morsilli, M. and **Bosellini, A.** (1997). Carbonate facies zonation of the Upper Jurassic-Lower Cretaceous Apulia Platform margin (Gargano Promontory, southern Italy). *Rivista Italiana di Paleontologia e Stratigrafia.* Milano. **103**, 193-206.

Morsilli, M., Hairabian, A., Borgomano, J., Nardon, S., Adams, E. and **Gartner, G.B.** (2017) The Apulia Carbonate Platform—Gargano Promontory, Italy (Upper Jurassic–Eocene). *AAPG Bull*., **101**, 523–531.

Moscardelli, L., Wood, L. and **Mann, P.** (2006) Mass-transport complexes and associated processes in the offshore area of Trinidad and Venezuela. *AAPG Bulletin*, **90**, 1059–1088.

Moscardelli, L. and **Wood, L.** (2008) New classification system for mass transport complexes in offshore Trinidad. *Basin Research*, **20**, 73-98**.**

Moscardelli, L. and **Wood, L.** (2015) Morphometry of mass-transport deposits as a predictive tool. *Geological Society of America Bulletin,* **128***,* 47-80.

Mutti, E., Carminatti, M., Moreira, J.L.P. and **Grassi, A.A.** (2006) Chaotic deposits: examples from the Brazilian offshore and from outcrop studies in the Spanish Pyrenees and Northern Apennines, Italy. *AAPG Annual Meeting, April 9–12*, Houston, Texas.

Mulder, T., Ducassou, E., Eberli, G.P., Hanquiez, V., Gonthier, E., Kindler, P., Principaud, M., Fournier, F., Leonide, P., Billeaud, I., Marsset, B., Reijmer, J.J.G., Bondu, C., Joussiaume R. and **Pakiades, M. (2012)** New insights into the morphology and sedimentary processes along the western slope of Great Bahama Bank. *Geology*, **40**, 603–606.

Odonne, F., Callot, P., Debroas, E.J., Sempere, T., Hoareau, G. and **Maillard, A.** (2011) Soft sediment deformation resulting from submarine sliding, favourable conditions and triggering mechanisms in examples from Eocene Sobrarbe delta (Ainsa, Spanish Pyrenees) and Cretaceous Ayabacas formation (Andes of Peru). *Sedimentary Geology,* **235**, 234–248.

Ogata K., Mutti, E., Pini, G.A. and **Tinterri, R.** (2012) Mass transport-related stratal disruption within sedimentary mélanges: examples from the northern Apennines (Italy) and south-central Pyrenees (Spain). *Tectonophysics,* **568–569**, 185–199.

Ogata, K., Pogačnik, Ž., Pini, G.A., Tunis, G., Festa, A., Camerlenghi, A. and **Rebesco, M.** (2014) The carbonate mass transport deposits of the Paleogene Julian-Slovenian Basin (Italy/Slovenia): internal anatomy and inferred genetic processes. *Marine Geology*, **356**, 88–110.

Ortiz-Karpf, A., Hodgson, D.M., Jackson, C.A.-L. and **McCaffrey, W.D.** (2017) Mass-transport complexes as markers of deep-water fold-and-thrust belt evolution: insights from the southern Magdalena Fan, offshore Colombia. Basin Research

Ortner, H. and **Kilian, S.** (2016) Sediment creep on slopes in pelagic limestones: Upper Jurassic of Northern Calcareous Alps, Austria, *Sedimentary Geology*, **334**, 350-363.

Owen, G., Moretti, M. and **Alfaro, P.** (2011) Recognising triggers for soft-sediment deformation: current understanding and future directions. *Sedimentary Geology*, **235**, 133-342.

Pickering, K.T. (1987) Wet-sediment deformation in the Upper Ordovician Point Leamington Formation: an active thrust-imbricate system during sedimentation, Notre Dame Bay, north-central Newfoundland. In: *Deformation of Sediments and Sedimentary Rocks* (Eds M.E. Jones, and R.M.F. Preston) *Geological Society of London, Special Publication,* **29**, 213–239.

Pickering, K.T. and **Corregidor, J.** (2005) Mass-transport complexes (MTCs) and tectonic control on basin-floor submarine fans, Middle Eocene, south Spanish Pyrenees. *Journal of Sedimentary Research*, **75**, 761–783.

Pieri, M. and **Mattavelli, L.** (1986) Geologic framework of Italian Petroleum resources: *AAPG Bulletin*, **70**, 103–130.

Playford, P.E., Hocking, R.M. and **Cockbain, A.E.** (2009) Devonian reef complexes of the Canning Basin, Western Australia. *Geological Survey of Western Australia, Bulletin*, **145**, 444.

Posamentier, H.W. and **Martinsen, O.J.** (2011) The character and genesis of submarine mass-transport deposits: insights from outcrop and 3D seismic data in Craig Shipp. In: *Mass Transport Deposits in Deep-Water Settings* (Eds R.P. Weimer and H.W. Posamentier), *SEPM Special Publication,* **96**, 7–38.

Principaud, M., Mulder, T., Gillet, H. and **Borgomano, J.** (2015) Large-scale carbonate submarine mass-wasting along the northwestern slope of the Great Bahama Bank (Bahamas): morphology, architecture, and mechanisms. *Sedimentary Geology.*, **317**, 27–42.

Safadi, M., Meilijson, A. and **Makovsky, Y.** (2017) Internal deformation of the southeast Levant margin through continued activity of buried mass transport deposits, *Tectonics*, 36, doi:10.1002/2016TC004342.

Simo, J.A., Scott, R.W. and **Masse, J.P.** (1993) Cretaceous carbonate platform: an overview. In: *Cretaceous Carbonate Platform* (Ed. T. Simo), AAPG Mem. **56**,1-14.

Schlumberger Market Analysis (2007) Schlumberger Market Analysis

www.slb.com (2007)

Skelton, P.W. (1991) Morphogenetic versus environmental cues for adaptive radiations.

In: *Constructional Morphology and Evolution* (Eds N. Schmidt-Kittler and K. Vogel), pp. 375–388.

Springer-Verlag, Berlin, Heidelberg.

Skelton, P.W. and Gili, E. (2012) Rudists and carbonate platforms in the Aptian: a case study on biotic interactions with ocean chemistry and climate. Sedimentology, 59, 81-117.

Sobiesiak, M.S., Kneller, B., Alsop, G.I. and **Milana, J.P.**, (2016) Inclusion of substrate blocks within a mass transport deposit: a case study from Cerro Bola, Argentina. In: *Submarine Mass Movements and Their Consequences* (Eds G. Lamarche, J. Mountjoy, S. Bull, T. Hubble, S. Krastel, E. Lane, A. Micallef, L. Moscardelli, C. Mueller, I. Pecher and S. Woelz), pp. 487-496. Springer International Publishing, The Netherlands.

Spalluto, L. and **Pieri, P.** (2008) Carta Geologica delle unita carbonatiche mesozoiche e cenozoiche del Gargano sud-occidentale: nuovi vincoli stratigrafici per l'evoluzione tettonica dell'area. *Mem. Descr. Carta Geol.* (d'It., LXXVII).

Stampfli, G.M. and **Kozur, H.W.** (2006) Europe from the Variscan to the Alpine cycles. In: *European Lithosphere Dynamics* (Eds D.G. Gee and R.A. Stephenson), Geological Society of London, Memoir **32**, 57-82.

Strachan, L.J. (2002) Slump-initiated and controlled syndepositional sandstone remobilization; an example from the Namurian of County Clare, Ireland. *Sedimentology*, **49,** 25-41**.**

Strachan, L.J. (2008) Flow transformations in slumps: a case study from the Waitemata Basin, New Zealand. *Sedimentology* **55**, 1311–1332.

Strachan, L.J. and **Alsop, G.I.** (2006) Slump folds as estimators of paleoslope: a case study from the Fisherstreet Slump of County Clare, Ireland. *Basin Research*, **18**, 451–470.

Van Der Merwe, W.C., Hodgson, D.M. and **Flint, S.S.** (2009) Widespread syn-sedimentary deformation on a muddy deep-water basin-floor: the Vischkuil Formation (Permian), Karoo Basin, South Africa. *Basin Research*, **21**, 389–406.

Van Der Merwe, W.C., Hodgson, D.M. and **Flint, S.S.** (2011) Origin and terminal architecture of a submarine slide: a case study from the Permian Vischkuil Formation, Karoo Basin, South Africa. *Sedimentology*, **58**, 2012–2038.

Winterer, E. L., Metzlery, C.V. and **Sarti, M.** (1991) Neptunian dykes and associated breccias (Southern Alps, Italy and Switzerland): role of gravity sliding in open and closed systems. *Sedimentology* 38, 381-404.

Yang, F., Zou, C., Hou, L., Yu, X. and **Li, S.** (2013) Hydrocarbon distribution and accumulation model in the south of Lixian slope, Raoyang subbasin. *Journal of Earth Science*, **24**, 1033-1043.

Zampetti, V., Schlager, W., Van Koninjenburg, J. and **Everts, A.** (2004) 3-D seismic characterization of submarine landslides on a Miocene carbonate platform: Luconia Province, Malaysia. *Journal of Sedimentary Research,* **74**, 817-830.

Zappaterra, E. (1990) Carbonate paleogeographic sequences of the Peri-Adriatic Region. *Bulletin of the Geological Society of Italy*, **109**, 5-20.

Unit	Interpreted type of MTD	Minimal lateral extent	Minimal height	Basal surface	Top surface	Subunits Thickness	Clast size	Interface contact
VGN 1	*Coherent slump*	*300 m*	*2.5 m*	*Erosional, bed-parallel*	*Depositional*	*N/A*	*N/A*	*N/A*
VGN 2	*Coherent to semi-coherent slump*	*600 m*	*4.0 m*	*Bed-parallel*	*Depositional*	*N/A*	*N/A*	*N/A*
VGN 3	*Debrite*	*500 m*	*1.5 m*	*Bed-parallel, slightly eroded*	*Depositional*	*N/A*	*Millimetres – 0.5 m; chert nodule size 0.05 – 0.2 m*	*N/A*
VGN 4	*Incoherent slump*	*500 m*	*8.0 m*	*Bed-parallel, lined by chert strata*	*Erosional, first bed chert layer*	*N/A*	*N/A*	*N/A*
VGN 5	*Debrite to incoherent slump*	*900 m*	*25.0 m*	*Bed-parallel*	*Depositional*	*3 – 10 m 15 – 20 m*	*Millimetres – 1.5 m; chert nodule size 0.05 – 0.3 m*	*Gradual (S) to sharp (N)*
VGN 6	*Debrite to incoherent slump*	*500 m*	*8.0 m*	*Deep erosional surface and bed parallel*	*N/A*	*N/A*	*Millimetres – 1.5 m; chert nodule size 0.05 – 0.3 m*	*Chaotic*
VGN 7	*Slide to coherent slump*	*>100 m*	*>10.0 m*	*Erosional*	*N/A*	*N/A*	*N/A*	*N/A*

	Interpreted type of MTD	Minimal lateral extent	Minimal height	Basal surface	Top surface	Interface contact
MTB 1	*Coherent slump*	*>20 m*	*1.0 m*	*Erosional, bed-parallel*	*Depositional*	–
MTB 2	*Coherent to semi-coherent slump*	*>25 m*	*1.25 m*	*Bed-parallel, slightly eroded*	*Depositional*	–
MTB 3	*Debrite to incoherent slump*	*>60 m*	*10.0 m*	*Bed-parallel, slightly eroded*	*Erosional, first bed chert layer*	–
MTB 4	*Debrite to incoherent slump*	*>10 m*	*1.0 m*	*Bed-parallel*	*Erosional*	–
MTB 5	*Coherent slump*	*>50 m*	*6.0 m*	–	–	–
MTB 6	*Debrite*	*450 m*	*10.0 m*	*N/A*	–	–
MTB 7	*Incoherent slump*	*>50 m*	*2.0 m*	*Bed-parallel*	–	–
MTB 8	*Debrite to incoherent slump*	*>15 m*	*3.0 m*	*Bed-parallel*	–	–
MTB 9	*Incoherent slump*	*>15 m*	*>5.0 m*	*Bed-parallel*	–	–

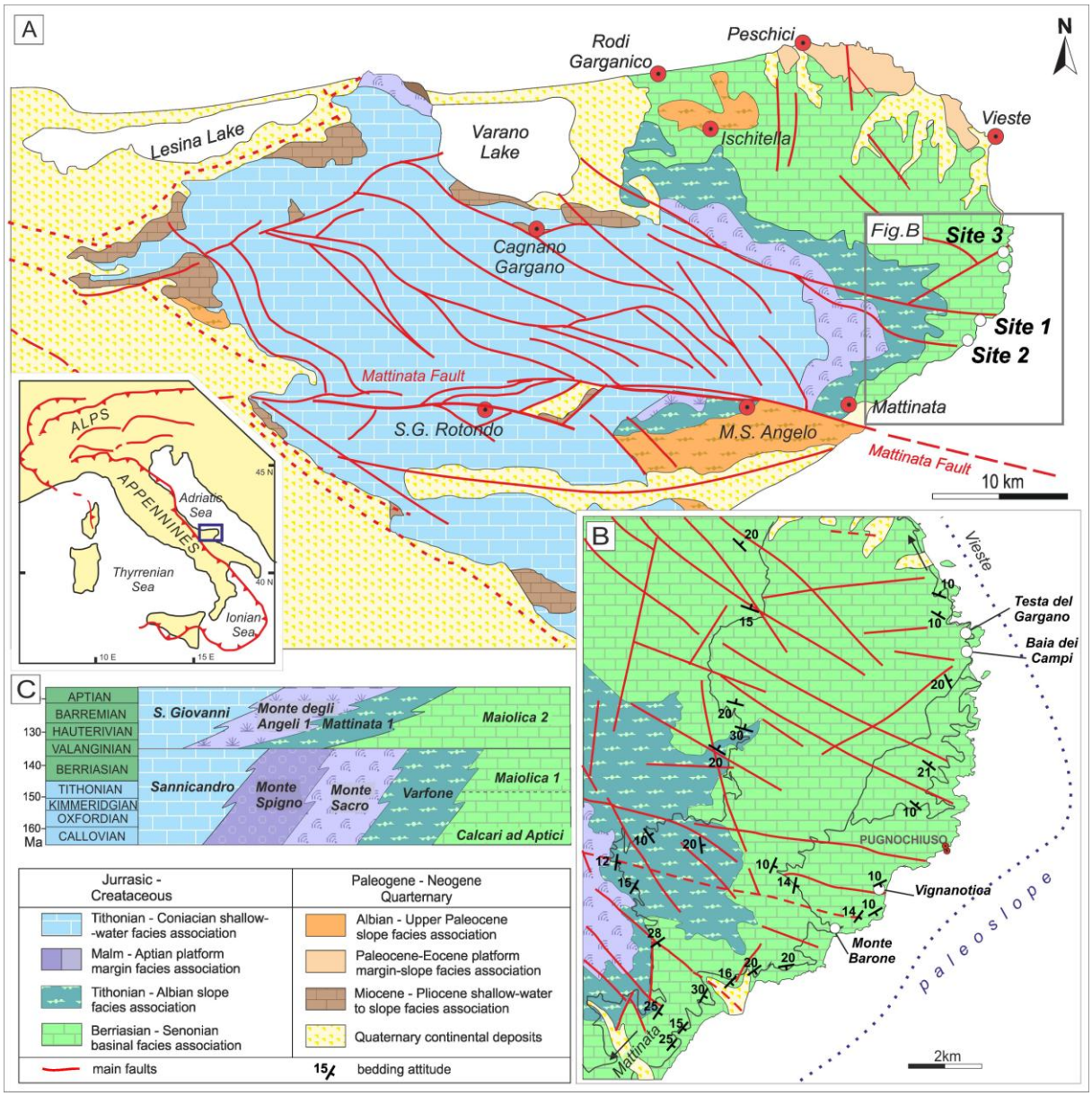

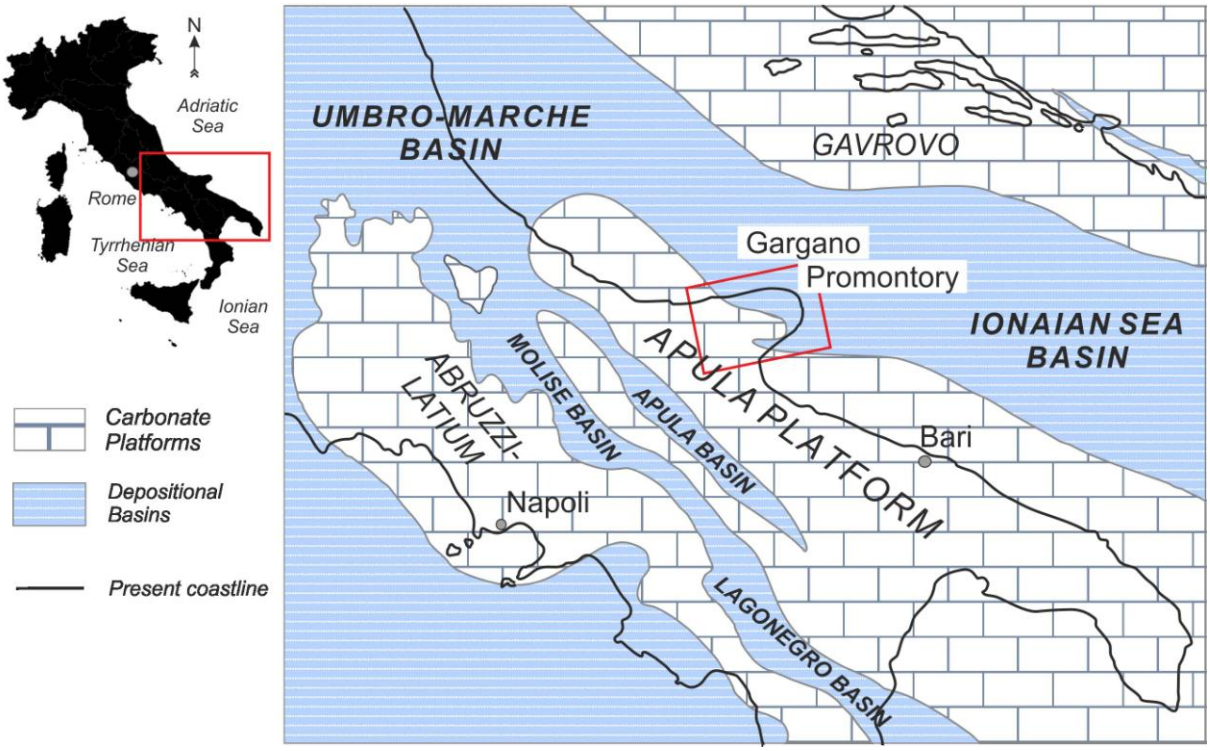

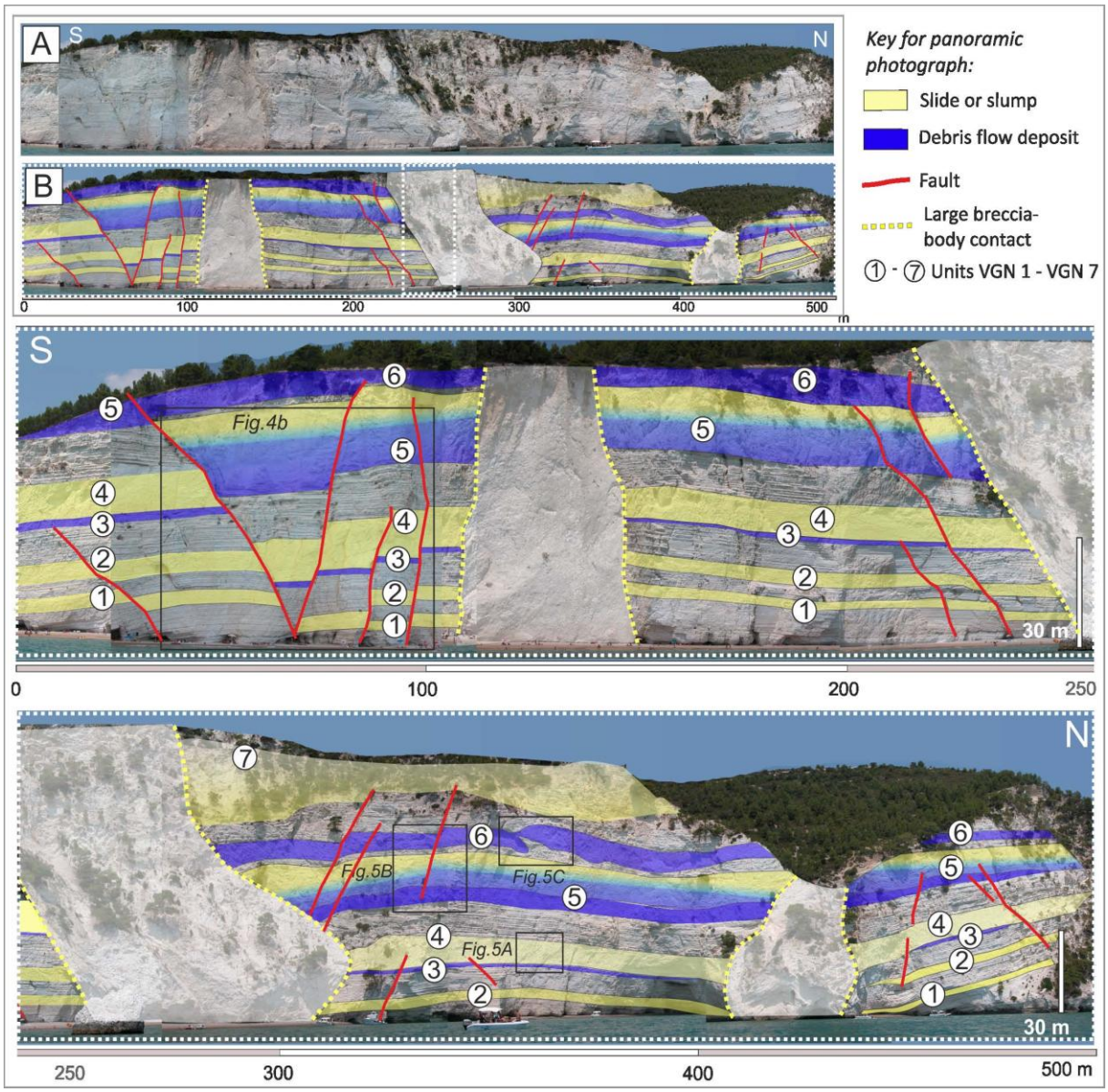

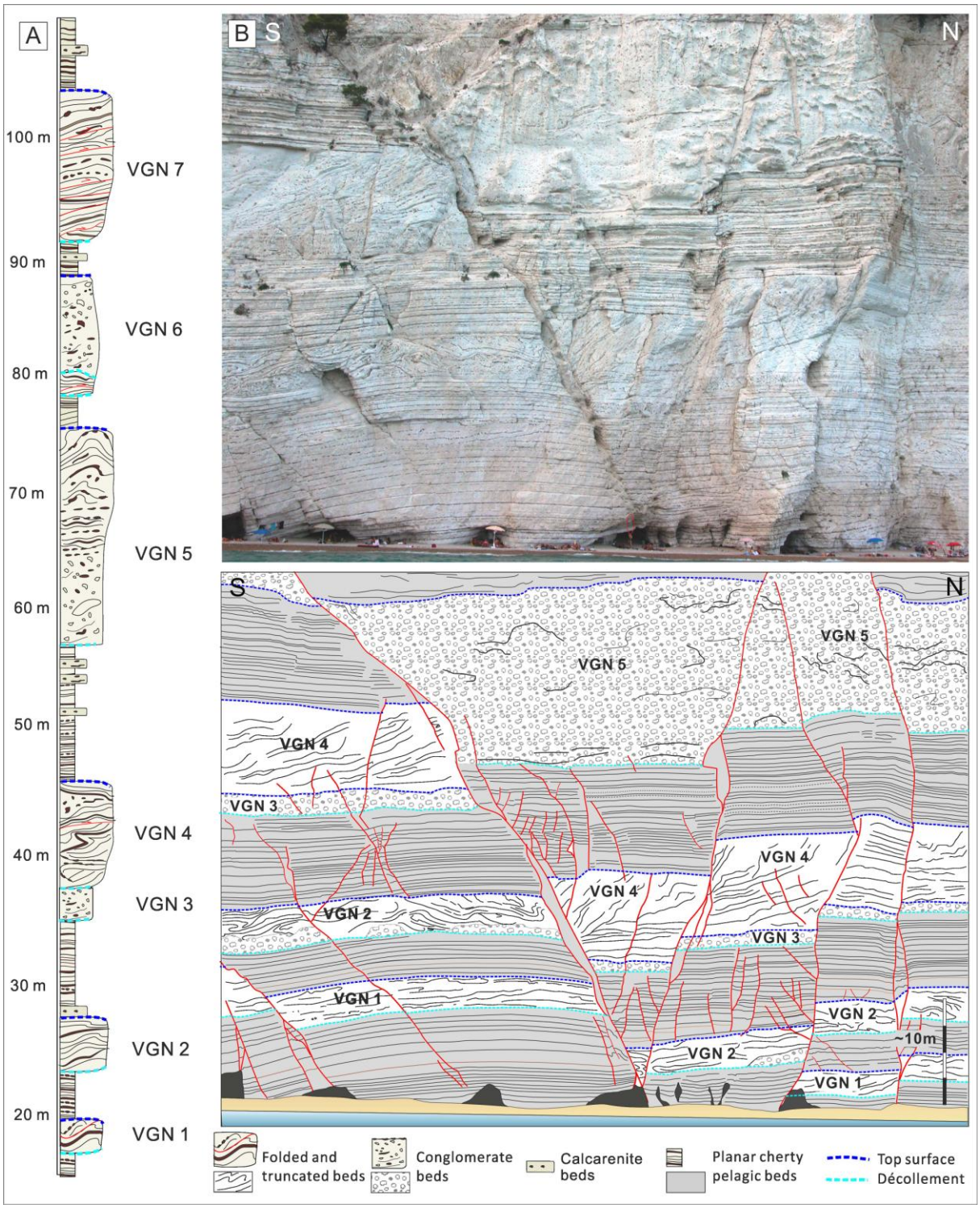

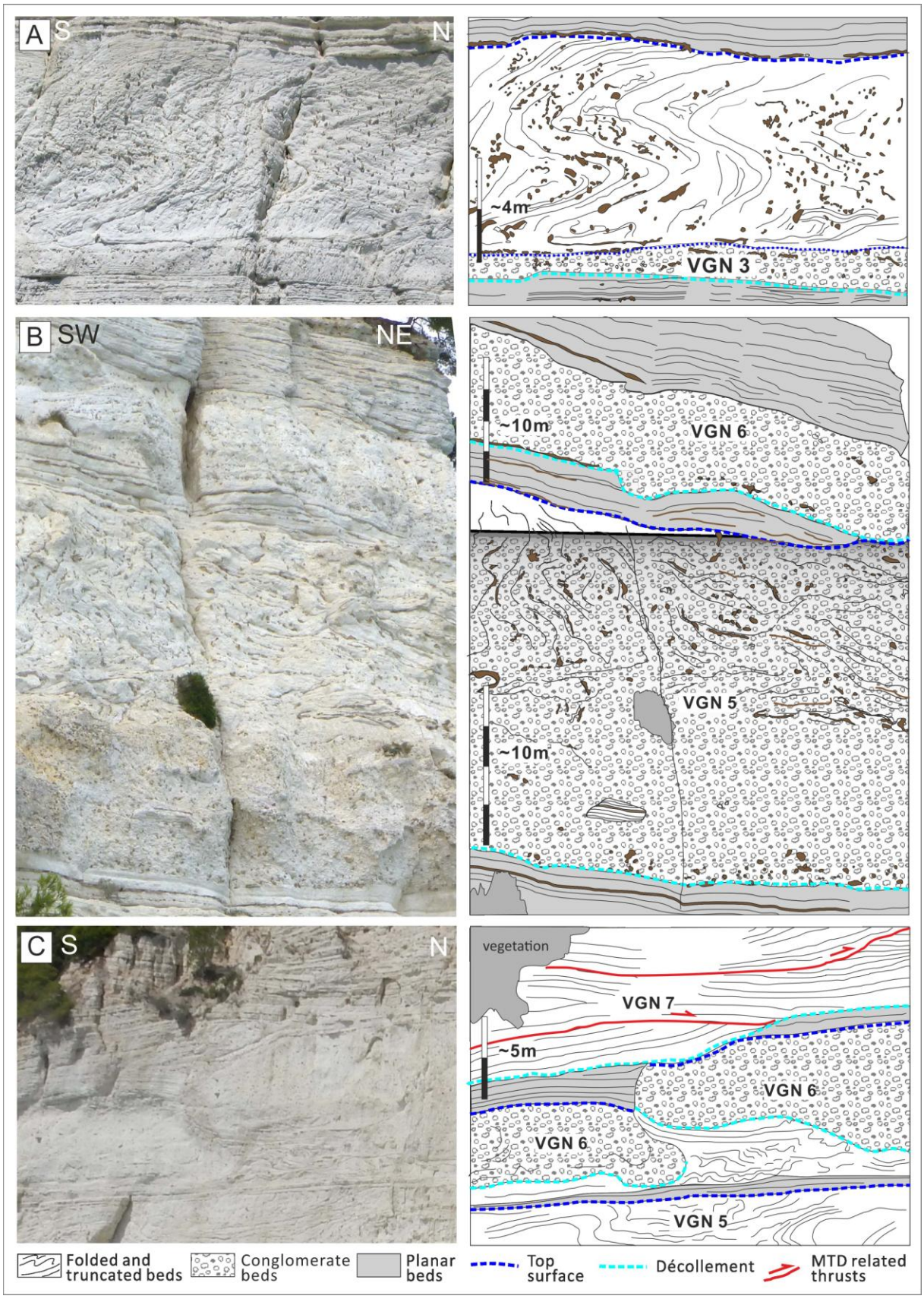

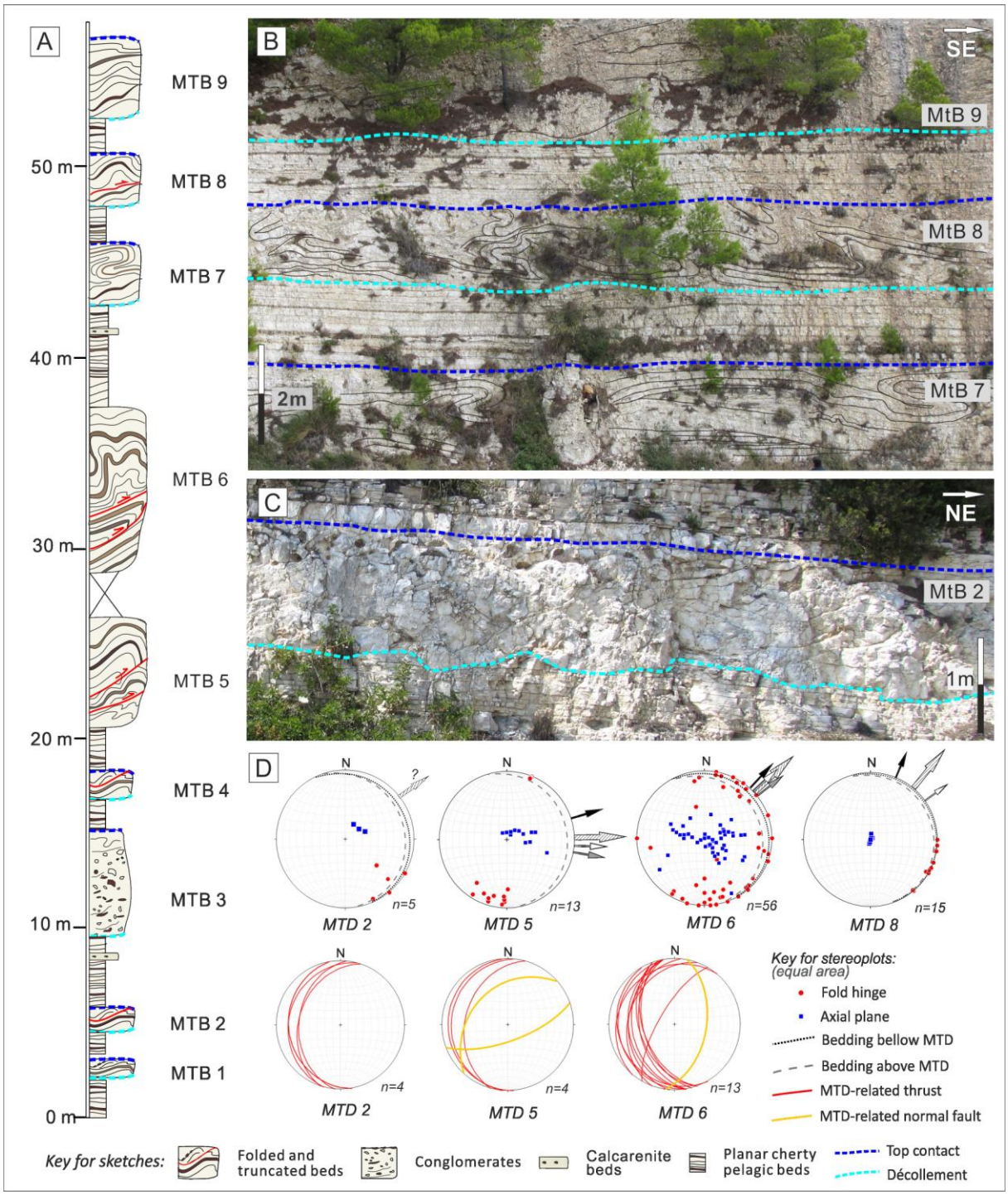

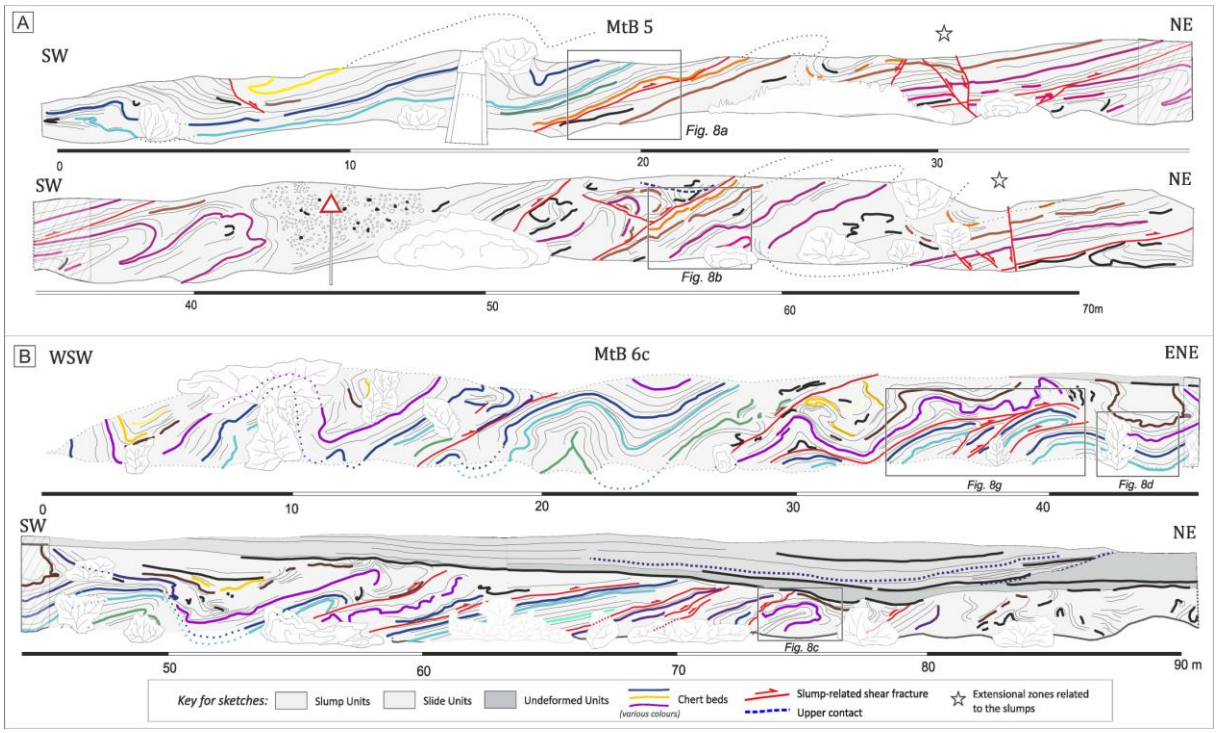

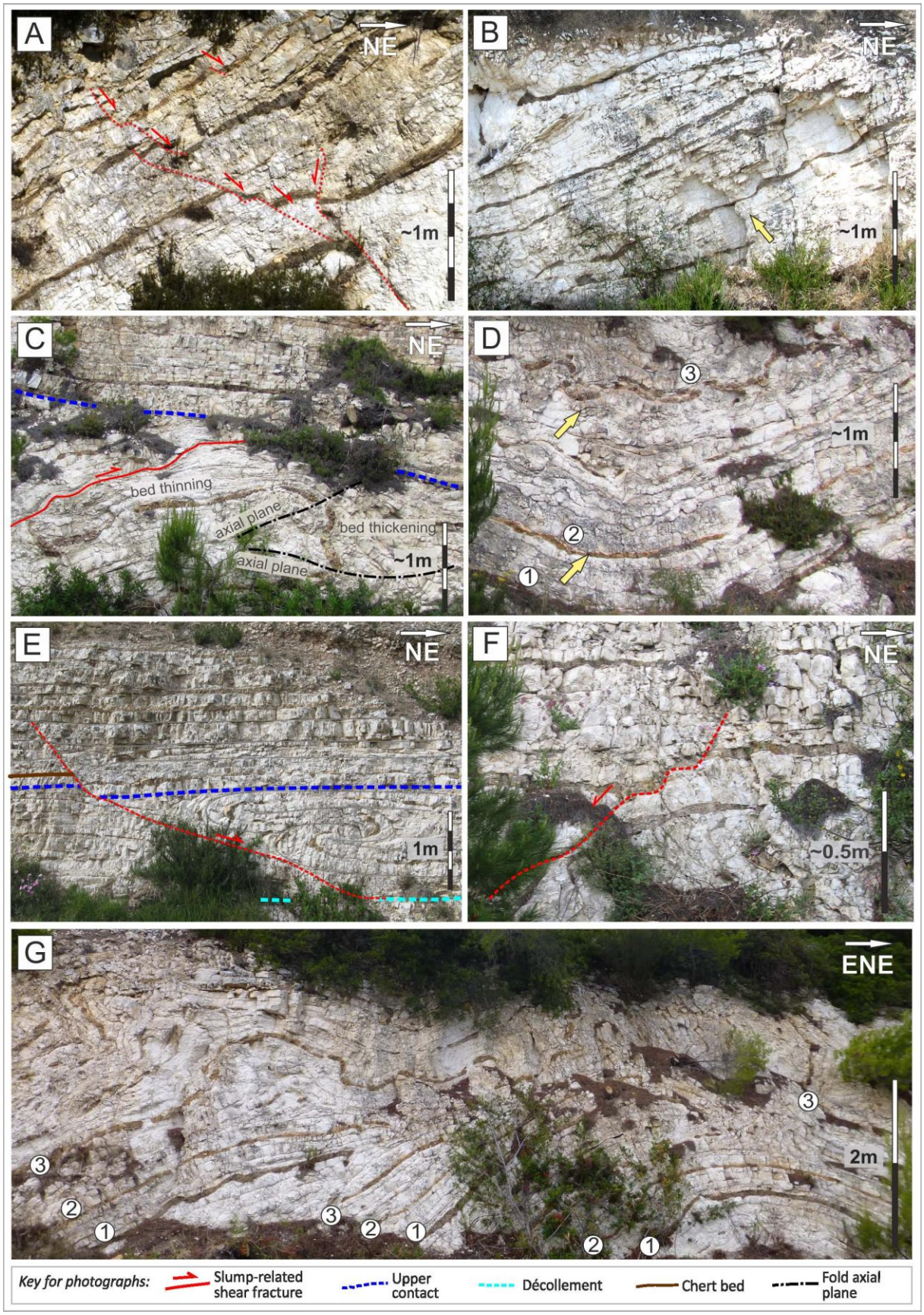

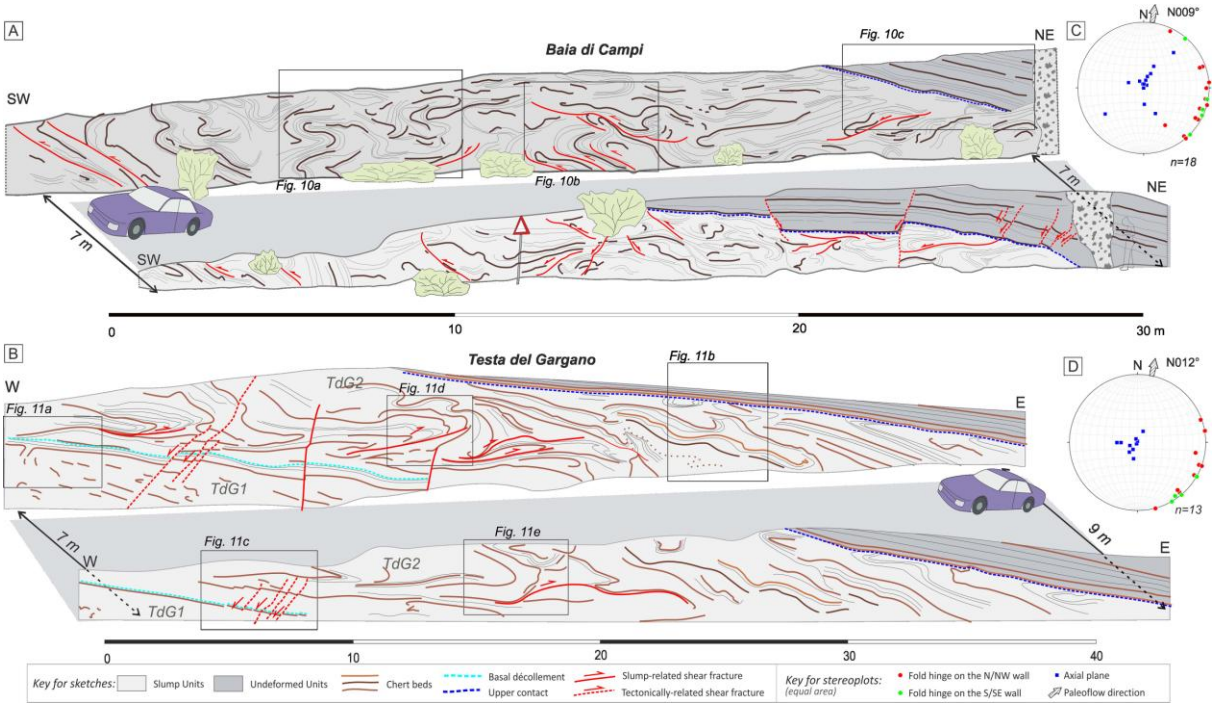

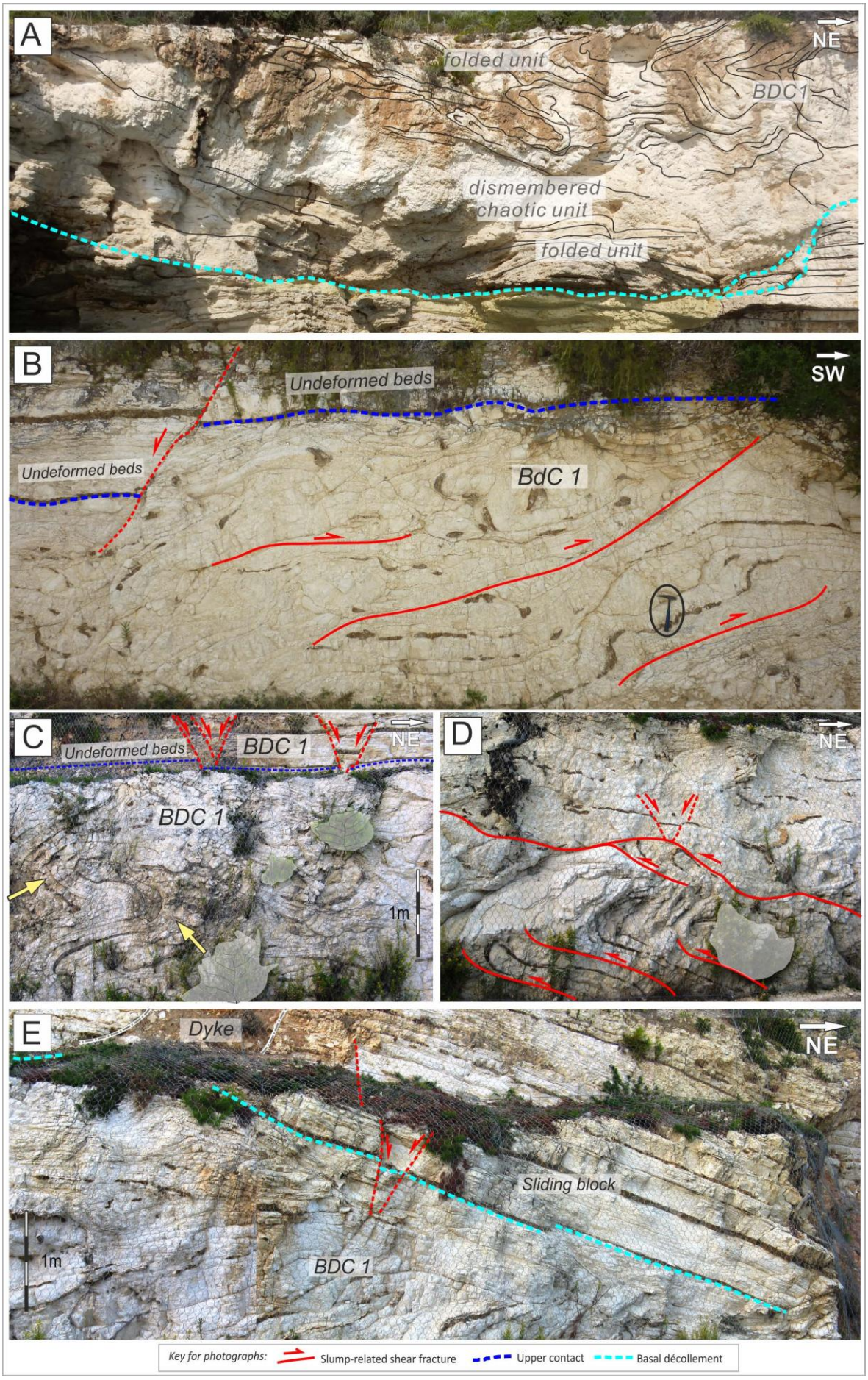

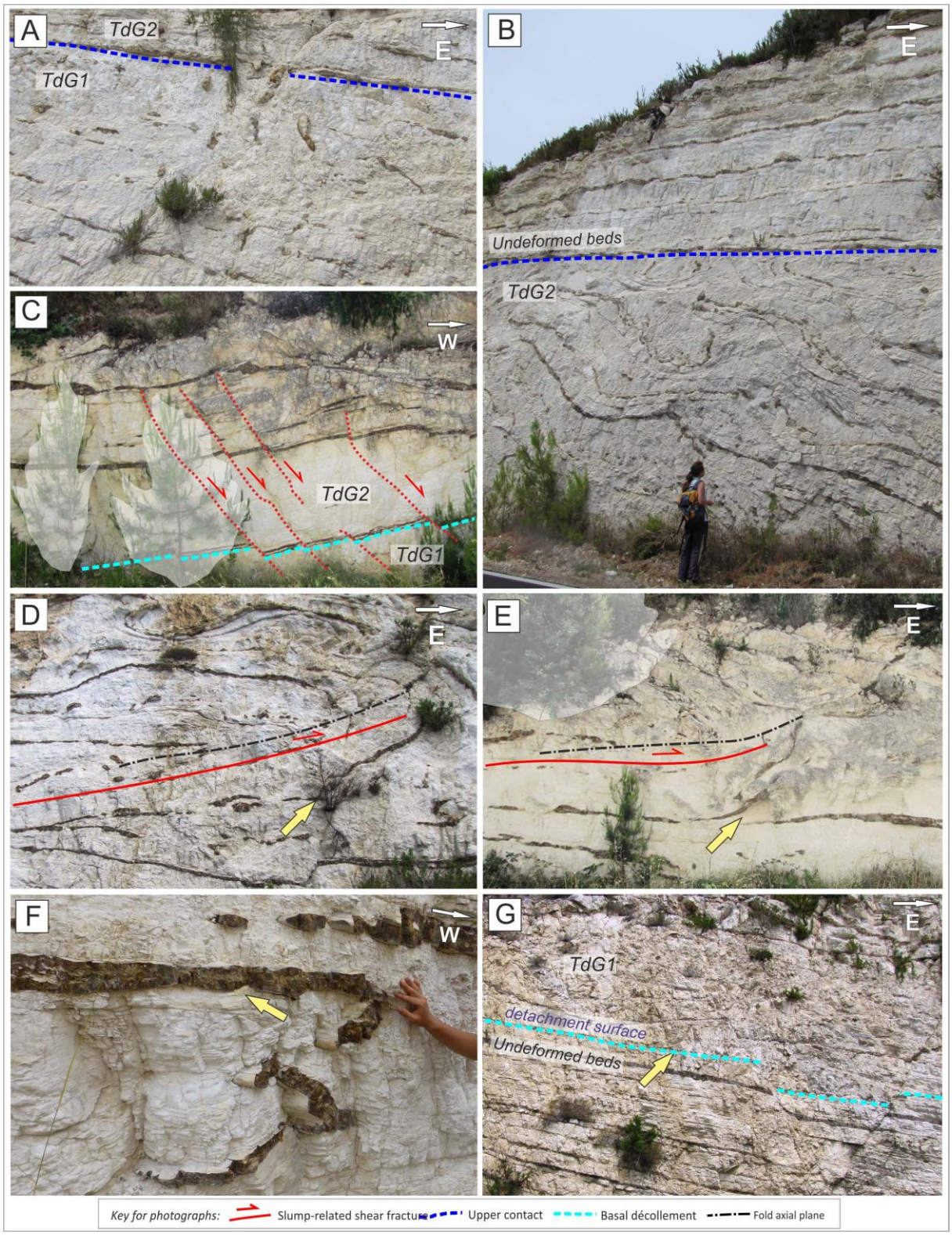

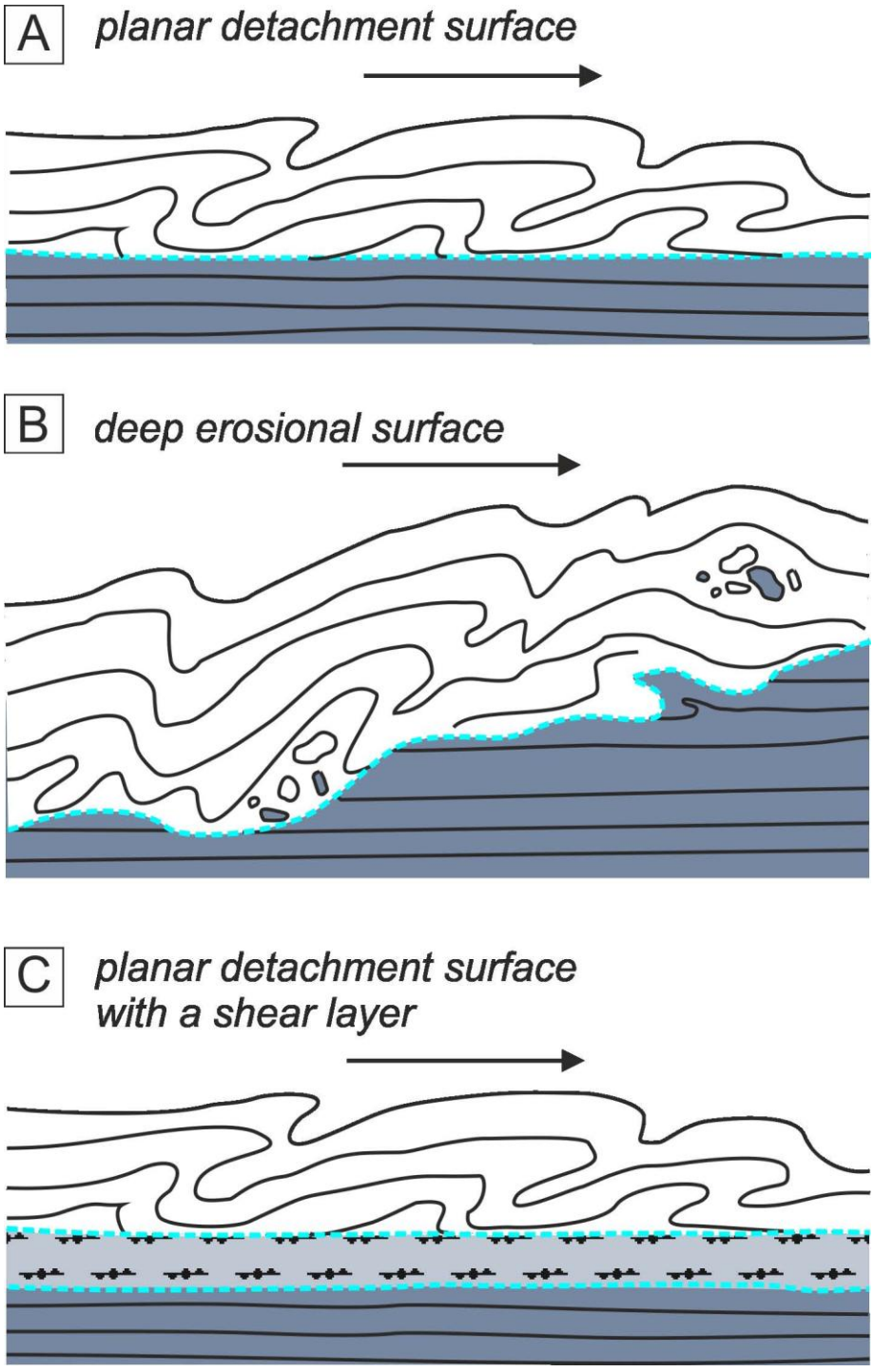

A *sharp sub-unit boundary*

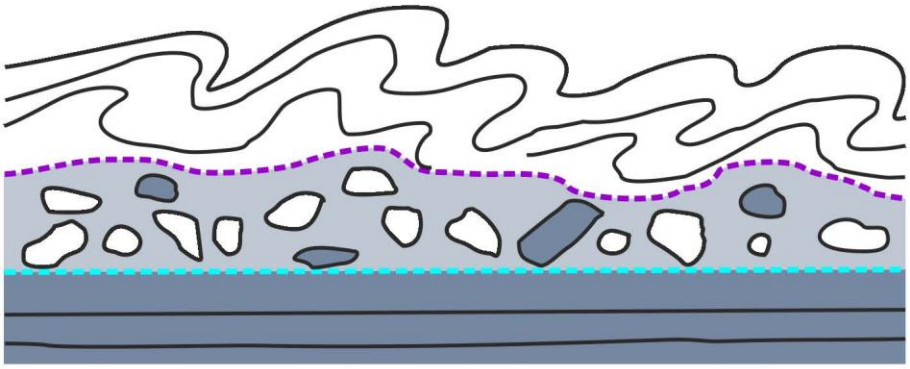

B *sharp deep-incised sub-unit boundary*

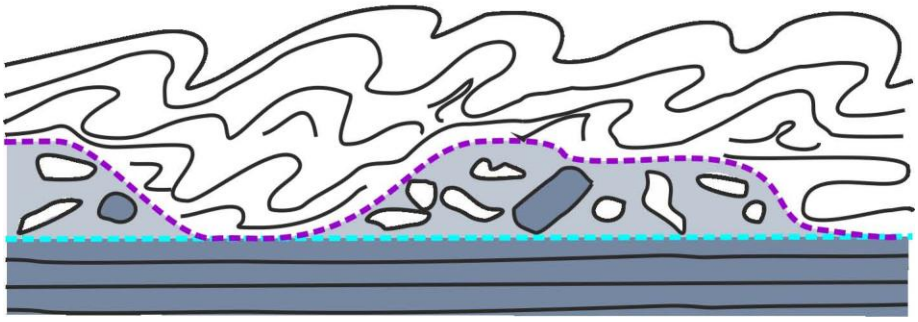

C *gradual sub-unit boundary*